Journal of Hydrology 624 (2023) 129897

Contents lists available at ScienceDirect

Journal of Hydrology

journal homepage: www.elsevier.com/locate/jhydrol

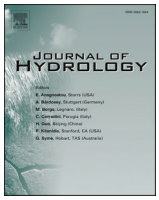

Research papers

Assessing hydrological sensitivity to future climate change over the Canadian southern boreal forest

Zhihua He *, John W. Pomeroy

Centre for Hydrology, University of Saskatchewan, Saskatoon S7N 1K2, Canada

ARTICLE INFO

This manuscript was handled by N. Basu, Editor-in-Chief, with the assistance of Andrea E. Brookfield, Associate Editor

Keywords:
Canadian southern boreal forest
Virtual basin modelling
Climate change
Pronounced spatial variability in hydrological sensitivity
Higher water yield region in the future

ABSTRACT

This study develops a physically based hydrological process model using the Cold Region Hydrological Modelling (CRHM) platform to simulate the water budget storages and fluxes over the Canadian southern boreal forest (SBF). Evaluation of the CRHM-based model in a well-gauged SBF basin, White Gull Creek (WGC), Saskatchewan, Canada, indicated quite good performance in reproducing historical observations of streamflow, snow water equivalent (SWE), evapotranspiration (ET) and soil moisture without parameter calibration from streamflow. The entire SBF was then evenly divided into 2243 virtual basins, each of which was structured and parameterized with the same land cover, soil and hydrological parameters as the WGC basin, but with local latitude and topography in order to examine the sensitivity of governing hydrological processes to future climate variability and perturbation. Hydrological sensitivity in the virtual basins was assessed by examining the differences between hydrological simulations driven by 4-km gridded convection-permitting Weather Research and Forecasting (WRF) outputs in the current period (ctrl, 2001–2013) and a Pseudo Global Warming period (pgw, 2087–2099). The WRF simulation in the pgw period was forced by a perturbation of the same boundary conditions from ERA reanalysis data as for the ctrl period, and the perturbation was based on the ensemble-mean of projected changes from the CMIP5 RCP 8.5 emission scenario. Results showed that temperature would increase by 4.5℃ to 7℃ over the SBF but increases in annual precipitation of 15–24% would more than compensate for the effects of warming on runoff generation and result in greater streamflow volumes. Annual streamflow volumes would increase by 64 mm (35%) and 95 mm (16%) in the west and east, and by 48 mm (17%) in the central SBF. Annual snowfall and maximum SWE would decrease by 89–109 mm (~29%) in the east, 3–8 mm (~6%) in the west, and 31–50 mm (~20%) in the central SBF. Annual mean soil moisture storage would decrease by 54–56 mm (27%) in the west and central, and by only 37 mm (14%) in the east SBF. Decreases in soil moisture would be caused by reduced soil freezing and enhanced thawing under future warming which would increase soil water loss from ET, subsurface runoff and percolation into groundwater storage. The larger sensitivity of streamflow and snow processes in the east SBF is partly due to the wetter climate and the larger increase in annual precipitation, the later also buffered the sensitivity of soil moisture to warming. These results show that the SBF would switch to a higher water yield region, dominated by rainfall-runoff fed streamflow over a longer snow-free season, and provide first-order guidance for sustainable water management of the SBF in the future.

1. Introduction

The boreal forest ecozone in Canada extends across a west-east band of around 5.5 million km^2, of which 49% is covered by trees, encompassing a variety of vegetation and climatic conditions (Matasci et al., 2018). Its hydrology provides crucially important freshwater and water-dependent resources, including rivers flowing north and south, for a globally important ecosystem and a local human population of around 3.7 million, including many Indigenous communities (Ireson et al., 2015). The boreal forest has been recognized as likely to be subject to relatively large degrees of climate warming by most global climate models (GCMs, Woo et al., 2008) and so its hydrology may be threatened by this change. Partly because of feedbacks from the reduced surface albedo associated with the shorter snowcovered period (Price et al., 2013), the boreal forest has recently experienced greater temperature warming than the global average trend. Changing temperature and precipitation are strongly impacting the processes of seasonal snow accumulation and melt and subsequent streamflow generation (Woo

* Corresponding author.
E-mail address: zhh624@mail.usask.ca (Z. He).

https://doi.org/10.1016/j.jhydrol.2023.129897
Received 27 January 2023; Received in revised form 6 June 2023; Accepted 29 June 2023
Available online 1 July 2023

et al. 2008), and primary productivity of terrestrial vegetation in this region (Nelson et al., 2014). The most threatened part of the boreal forest in Canada is its southern section, as water use from agriculture, mining and municipal water supply are concentrated here, and this is the southern edge of viability for this biome (Brandt et al. 2013). Improved understanding of how the changing climate impacts its hydrology, including individual hydrological processes, is thus critical to the sustainable management of the boreal forest (Ireson et al. 2015). However, assessment of hydrological sensitivity to climate change over the entire southern boreal forest (SBF) is rather rare, due to the limited availability of data for hydrological model setup and calibration, and the large uncertainty and errors in representing precipitation dynamics in climate projections from coarse-resolution climate models.

The boreal forest consists of multiple land cover types including lakes, wetlands, shrubs and trees. Forested areal fractions can exceed 60% in many locations (Brandt, 2009), and are dominated by species of white and black spruce, aspen, jack and lodgepole pine, balsam fir and poplar (Luke et al., 2007; Matasci et al. 2018). Thus, tree canopy plays a critical role in the partitioning of water and energy in the boreal forest (Pomeroy et al., 1999). For instance, snowfall comprises 20–40% of annual precipitation in the boreal forest (Ireson et al. 2015), however, 30–40% of this can be lost by sublimation of snow intercepted in the canopy (Pomeroy and Schmidt, 1993; Pomeroy and Gray, 1995; Hedstrom and Pomeroy, 1998; Pomeroy et al., 1998a). Canopy interception losses typically result in 20–45% lower snow water equivalent (SWE) under dense canopies compared to adjacent clearing (Pomeroy et al., 2002). The forest canopy also strongly alters radiant and turbulent energy transfer to sub-canopy snow surface, reducing melt rates compared to open environments (Harding and Pomeroy, 1996; Pomeroy and Granger, 1997). Greater canopy densities result in reduced short-wave radiation because of shading but enhanced longwave irradiation from the forest thermal emissions (Sicart et al., 2004; Pomeroy et al., 2009; Essery et al. 2008; Ellis et al., 2011). Turbulent energy fluxes under the forest canopy are greatly reduced due to dampened wind speed and turbulence (Harding and Pomeroy, 1996). Robust estimations of snow accumulation and melt under boreal forest canopies requires a physically based hydrological process model that includes the effect of forest canopies on mass and energy exchanges and consideration of frozen soil effects on infiltration and soil water availability (Gelfan et al., 2004).

The Cold Regions Hydrological Model (CRHM) contains a canopy module that couples canopy processes of snow interception, unloading, sublimation and drip, and energy flux exchanges through the canopy between atmosphere and snow surface (Pomeroy et al., 1998a, b; Pomeroy et al. 2007, 2022; Ellis et al. 2010). The model has been successfully applied to reproduce the major hydrological processes and predict hydrology changes under changing climate in a wide range of cold regions including mountains (Fang and Pomeroy, 2020; Pomeroy et al., 2016; Zhou et al., 2014; López-Moreno et al., 2013), prairies (Armstrong et al., 2015), taiga and tundra (Krogh et al., 2017), and boreal forest (Ellis et al. 2010; He et al., 2021). It generally performed very well in simulating the snowpack regime and soil moisture under the forest canopy, calculating the yearly water budget, and in synthesizing streamflow in forested basins with no calibration of model parameters (Ellis et al. 2010; Pomeroy et al., 2012; Rasouli et al., 2014).

However, setting up CRHM to simulate large areas of boreal forest is challenging, because drainage networks are particularly uncertain in northern Canada due to the widely distributed wetlands and lakes and ephemeral streams (La Roi, 1992). Similar issues occur in the poorly drained Canadian Prairies because of the extensive depressions (wetlands) and variable connectivity between them (Shook and Pomeroy, 2011). Armstrong et al. (2015) thus adopted a virtual basin approach to model the spatial variability of ET across the entire Canadian Prairies. In their approach, each site location within the study region was treated as a uniform exemplary drainage basin, called a virtual basin, which is composed of the primary land cover, drainage and soil units called hydrological response units (HRU). They used a simple CRHM-based model to standardize the basin representation of lateral water redistribution over a vast region. López-Moreno et al. (2020, 2021) and Spence et al. (2022a) extended this virtual basin approach to represent global mountain and Prairie wetland hydrology respectively, covering large areas. Their successes suggest that the virtual basin modelling approach may be suitable for mapping the spatial variability of hydrological sensitivity across a large boreal forest region.

Climate scenarios projected by global and regional climate models (GCMs and RCMs) can be effective forcing for hydrological models to assess future hydrology (Weber and Flannigan, 1997). Nonetheless, the spatial resolutions of most GCMs and RCMs are too coarse to represent the mixed surface fluxes from forest, wetland and lakes and the deep convection processes in the atmosphere (Li et al., 2019), which typically result in large convective storms during the boreal forest summer (Price et al., 2013). Recently, a high-resolution (4 km) convection-permitting module (CPM) has been integrated into the WRF model to resolve deep convection processes and estimate the corresponding convective storms (Liu et al., 2017). Assessments of the CPM indicated its good performance in providing precipitation estimates to balance the surface water budget for continental-scale Canadian river basins (Kurkute et al., 2020) and in estimating the reliance of summer weather on soil moisture over the contiguous US (Zhang et al., 2020). The WRF-CPM appears to provide the highest resolution for future climate over the Canadian boreal forest amongst available climate models. However, the value of WRF-CPM data for investigating hydrological sensitivity to climate changes in the Canadian boreal forest has not been investigated.

This study therefore proposes to evaluate hydrological sensitivity to future climate change over the SBF using a virtual basin modelling approach. Virtual basins were parameterized by the physically based CRHM across the entire SBF without calibration, and were thus less impacted by data availability in the study region. Near-surface meteorology from the high resolution WRF-CPM in two 13-year periods of current (2001–2013) and future (2087–2099 under climate change) provide one of the least uncertain sources of meteorological forcing to force each of the virtual basin models separately. The objectives of the study are to determine the spatial heterogeneity of (1) the sensitivities of annual ET and streamflow regimes; (2) the sensitivities of canopy snow interception and snow sublimation, snowpack and snowmelt, and snowcovered period; and (3) the sensitivities of soil freezing-thawing and sub-surface moisture, across the Canadian SBF. These sensitivities were evaluated using a fixed "exemplar" virtual basin representation, so as to focus on the impacts of variable and changing climate on hydrological processes and response. It is expected that the results will provide crucial information on the prospects of the water resources that support this biome and can inform sustainable forest management and conservation.

2. Study area and data

The Canadian SBF covers around 1.4 million km^2 and extends approximately 4000 km from the province of British Columbia in the west to the province of Newfoundland and Labrador in the east (Fig. 1). The SBF is featured by seasonally frozen soils but little permafrost (extent mapped using data from https://open.canada.ca/data) and is located within the Boreal Plains and Boreal Shield ecozones (Fig. 1a). The SBF covered by the WRF model area was used as the modelling area for this study (Fig. 1b). To explore regional differences in present and future hydrology, the modelling area was further divided by longitude into three parts: west (>100° W), central (80° W – 100° W) and east (<80° W). The west SBF (primarily Alberta and Saskatchewan) is in the Boreal Plains ecozone as classified by the National Ecological Framework for Canada (Ecological Stratification Working Group, 1996), while the central (primarily Manitoba and Ontario) and east (primarily Quebec) SBF are mainly in the Boreal Shield ecozone (Wong et al., 2017). Annual precipitation generally increases from west to east across the SBF. The current climate in west SBF is sub-humid with an annual

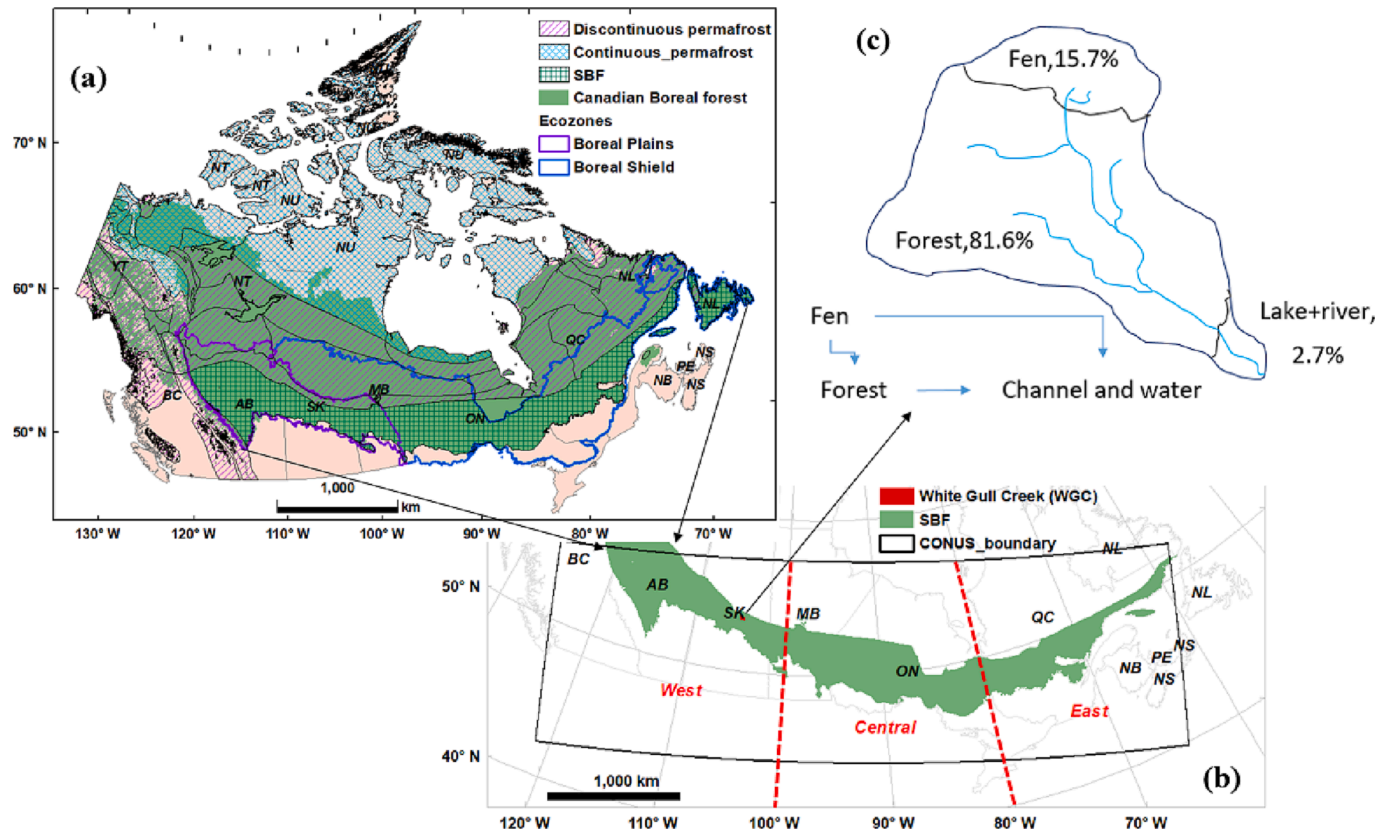

Fig. 1. (a) Delineation of the Canadian southern boreal forest (SBF). (b) SBF area located within the spatial coverage of WRF-CPM CONUS data. (c) HRUs and corresponding areal fractions, as well as their routing orders in the virtual basin. Red polygon in (b) refers to the location of the White Gull Creek basin (WGC). (For interpretation of the references to colour in this figure legend, the reader is referred to the web version of this article.)

precipitation of 300–625 mm, whilst that in the central and east SBF is humid with an annual precipitation of 400–1600 mm (Luke et al. 2007).

A benchmark, "exemplar" basin, defined by the drainage of White Gull Creek (WGC, 105° 9' W-104° 37' W; 53° 51' N-54° 7' N, 602 km^2), where hydrometeorological variables including precipitation, air temperature, wind speed, relative humidity, soil moisture and snowpack were intensely surveyed and gauged, was used for the verification of the hydrological model. The WGC basin is located in north-central Saskatchewan, north of the city of Prince Albert (Fig. 1b). This site was used by NASA and the Canadian Government to characterise the global southern boreal forest for the BOREAS land surface hydrometeorology experiment in the 1990s (Sellers et al., 1995 and 1997). The mean annual precipitation and air temperature measured during 1998–2016 in the basin were 440 mm and 1.5℃, respectively. WGC is 80% forest covered, with black spruce, jack pine and aspen being the main species (Barr et al., 2012). Snowfall comprises 30% of annual precipitation and winter is 6–7 months, and therefore snow processes govern much of the seasonal runoff generation because melt occurs when soils are frozen and with limited infiltration capacity (Pomeroy and Granger, 1997). Meteorological observations, soil and snow survey data on the forest site, as well as daily streamflow gauged at the basin outlet during 2001–2013 were used for the model evaluation (Sellers et al. 1997; Barr et al. 2012; Ahmed et al. 2020) and are described by He et al. (2021).

To investigate hydrological sensitivity to future climate perturbation, the WRF-CPM simulations over the contiguous United States and southern Canada (CONUS, Rasmussen and Liu. 2017; Liu et al. 2017) were used to force the hydrological model over the SBF. The WRF-CPM generated a unique high resolution (4 km) climate data over the entire SBF based on a convection-permitting module which explicitly represented deep convection and more accurately represented the underlying topography and land surface in the SBF (Li et al. 2019). The boundaries of WRF's CONUS coverage are shown in Fig. 1b and cover most of the SBF except for its eastern edge in Newfoundland and Labrador and northern edge in British Columbia. Near-surface outputs from the WRF-CPM CONUS runs including air temperature, precipitation, relative humidity and solar over the current scenario (ctrl, 2001–2013) and a future scenario using a Pseudo Global Warming approach for RCP 8.5 (pgw, 2087–2099) were used to force the hydrological model. In this approach, the ctrl simulation was driven by boundary conditions derived from ERA-Interim reanalysis data and a convection-permitting module (CPM) in WRF (Li et al. 2019). For the pgw simulation, the WRF-CPM model was forced by perturbations of the same boundary conditions from ERA reanalysis, with perturbations taken as the ensemble-mean projected changes in meteorological variables from the CMIP5 RCP 8.5 emission scenario. Both ctrl and pgw simulations were conducted at a spatial resolution of 4 km in the WRF-CPM model. The WRF runs were bounded by ERA-interim reanalysis data and so are similar to real meteorology over historical period, but with synthetic weather system dynamics produced by the WRF model. Its future pgw runs produce a credible future weather pattern including future convective precipitation dynamics that are useful for hydrological model forcing.

3. Methods

3.1. Cold regions hydrological model (CRHM)

The CRHM is an object-oriented flexible platform for assembling physically based process modules into a hydrological model (Pomeroy et al. 2007; 2022). The spatial discretization of study basin is based on the concept of HRUs which are typically classified by the combinations of land cover and terrain features (Krogh et al., 2015) and areas largely

correspond with landscape types in the SBF (Pomeroy et al., 1999). A range of CRHM modules for general hydrological modelling have been described in detailed in previous applications (e.g., Ellis et al., 2010; Fang et al., 2010, 2013; López-Moreno et al., 2013; Pomeroy et al., 2015; 2016). For hydrological modelling in SBF, the following main modules were used.

1. Canopy: this module characterizes the vegetation coverage of each HRU using parameters such as leaf area index (LAI), vegetation height, and the canopy snow loading capacity, and calculates the interception of snowfall and rainfall, sublimation and the unloading and drip from the forest canopy, as well as the sub-canopy snow accumulation, rainfall, and shortwave and longwave irradiance (Ellis et al., 2010).
2. Blowing snow: this module estimates redistribution of snow in open areas by wind transport amongst HRUs, as well as the snow sublimation losses (Pomeroy and Li, 2000).
3. Energy-balance snowmelt: the energy balance components of short- and long-wave irradiance, latent and sensible heat fluxes, rainfall advection, and the internal energy exchange between snowpack layers and the soil are calculated by this module (Marks et al., 1998). Snowmelt, sublimation and discharge from the snowpack are determined by the latent heat requirements for melt and sublimation and net energy availability.
4. Soil moisture: this module calculates detention layer, two soil layers and groundwater water storage, vertical transfer of moisture and horizontal subsurface and groundwater runoff using Darcy velocities adjusted for saturation and permeability (Fang et al., 2010; 2013; Pomeroy et al., 2016).
5. Soil freeze–thaw: the freezing and thawing fronts in soil and soil temperature are estimated in this module, based on the radiation-convection-conduction approach for the ground surface conditions when snow-free (Williams et al., 2015), snowpack energy balance and thermal conductivity in winter, and a modification of Stefan's heat flow equation for heat flow in soils (Changwei and Gough, 2013). Liquid water availability in soil layers is calculated based on location of the thawing and freezing fronts.
6. Infiltration: this module calculates infiltration of snowmelt into frozen soils using Gray's parametric infiltration algorithm (Gray et al., 2001), infiltration of rainfall to unfrozen soils by Ayers' infiltration expression (Ayers, 1959), and infiltration-excess overland runoff induced by snowmelt and rainfall.
7. Evaporation: this module uses the Priestley and Taylor evaporation expression (Priestley and Taylor, 1972) to estimate the actual evaporation from saturated surfaces such as wetlands, open water bodies and river channels, and uses the Penman-Monteith (P-M) algorithm (Monteith, 1965) with a Jarvis-style resistance formulation (Verseghy, 1991) to estimate the actual ET from unsaturated surfaces and wetted canopies. Meanwhile, this module updates moisture contents in the interception storage, depression storage and soil layers.
8. Routing: a Muskingum method (Chow, 1964) is used by this module to represent the routing of surface runoff between HRUs. Routing of subsurface and groundwater runoff is calculated using Clark's lag and route algorithm (Clark, 1945).

3.2. Parameterization of virtual basins in the boreal forest

Considering the common land cover and terrain patterns across the SBF, an upland virtual basin with three HRUs of fen, forest and open water, was set up for hydrological modelling (Fig. 1c). The fractional areas for Fen, Forest and Open Water (lakes and rivers) HRUs were estimated as 15.7%, 81.6% and 2.7%, respectively, based on land covers in the WGC basin. The Fen HRU in the virtual basin corresponds to shrub-covered wetlands in topographic depressions, which was treated as upland to lakes and rivers in the routing system (Fig. 1c). The Forest HRU was used to represent the canopy and transpiration functions in partitioning water and energy inputs played by multiple tree species such as spruce, pine, fir, poplars, and birch (La Roi, 1992). Pine (including Lodgepole Pine in the west, White Pine in the east, and Jack Pine over the SBF) was used as a representative tree over the SBF in the virtual Forest HRU, as it is extensively distributed in the SBF, typically has a high winter LAI and influences snow interception, sublimation, accumulation and melt processes as well as summer transpiration. To make the modelling approach comparable, identical tree species and land cover types were used across the SBF. Large lakes and large open sites dominated by exposed bedrocks or thin soil layers exist in the SBF, especially in the east, which, however, were not considered in the virtual basin as they are not common land covers in the central and west parts of the SBF and the focus of the study was on forest hydrology processes in upland basins. The virtual basin in this work was set up for regions which are dominated by trees or wetlands, so as to focus on the effects of interaction between climate change and forest canopy on hydrology in the SBF.

Forest parameters such as LAI, vegetation height, and snow load capacity for this HRU were estimated from values reported in local field studies (e.g., Chen et al., 1997; Pomeroy and Granger, 1997; Hedstrom and Pomeroy, 1998; Pomeroy et al. 1998a; Nijssen and Lettenmaier, 2002; Pomeroy et al. 2002; Barr et al. 2012). The mean winter effective LAI of 2.4 that is typical of pine was set for forest (Table 1), and LAI of 0.1 was assigned for the Fen and open water HRUs. Vegetation height has strong influences on boundary layer winds and hence for blowing snow; values of 11 m and 0.1 m were assigned for the Forest and Fen HRUs, respectively. Canopy snow load capacity indicating the maximum snow interception that the canopy can hold was set as 6 kg/m^2 for the Forest HRU (similarly in He et al. 2021). The blowing snow fetch distance parameter was set as 300 m for all the HRUs due to the short upwind distance. Storage capacity of groundwater reservoir was set as 200 mm.

Soil parameters such as layer depth and porosity of HRUs were estimated from the predominant soil texture in the WGC basin (Agriculture and Agri-Food Canada, 2015). Soil water storage capacity was calculated by multiplying soil depth with porosity. Similar to He et al. (2021), the model runs started from October 1st with an assumed saturated soil moisture in fall. Saturated hydraulic conductivities and pore size distributions were used from He et al. (2021), which were set from soil texture in the WGC basin. Soil temperature was initialized by ground surface temperature using the snowpack temperature and heat conduction or the radiation-convection-conduction approach in the soil freeze–thaw module. The model was spun up by running over two years, which helps to reduce the impact of initial conditions. It is worth noting that soils in the SBF vary from west to east; the dominant soil types are Luvisols and Brunisols in the west, changing to Podzols in the east. However, soil texture throughout the SBF is typically sandy and loamy, along with the generally existing glacial-Till (Maynard et al. 2014). CRHM uses the soil texture parameter to characterize the influence of soil type on hydrology. In the virtual basin, soil texture was set as loam for the Fen and Open Water HRUs, and was set as sand for the Forest HRU, which it is then assumed to represent the common soil texture across the SBF. Runoff from the Fen and Forest HRUs was routed into the third Open Water HRU and then to the basin outlet. Routing lengths of channels in HRUs were estimated by the GIS analysis of terrain in WGC. Manning's equation was adopted to estimate the mean streamflow

Table 1
Canopy parameters for HRUs in the virtual basin model.

HRU name	Open water and channel	Forest	Fen
Area (km^2)	17.0	510.1	97.8
LAI	0.1	2.4	0.1
Vegetation height (m)	0.001	11	0.1
Snow interception capacity (kg/m^2)	0	6	0

flowing rate based on longitudinal channel slopes of the HRUs that were calculated by DEM maps, using a Manning's roughness coefficient of 0.016 and hydraulic radius of 0.25 (He et al. 2021).

The entire SBF modelling area was evenly divided into 2243 grids, each with an area of around 625 km^2 (i.e., 25 × 25 km which is close to the area of WGC basin). Each grid was treated as a virtual basin that is composed of the representative land cover types. The mean latitude, longitude, slope, aspect and elevation of the virtual basins were set based on grid centroid properties determined from the ArcGIS maps. HRU area fractions and model parameters in the 2243 virtual basins were kept consistent to that of the WGC basin in order to standardize hydrological modelling over the SBF and focus analysis on the general spatial variability of hydrological sensitivity as forced by climate variability. The performance of CRHM set up in this configuration was evaluated by the fit between simulated streamflow, SWE, actual ET and volumetric water content (VWC) of soil liquid moisture during May-September, and the corresponding observations in the WGC basin over 2001–2013. For model evaluation in the WGC basin, the virtual basin model was forced by meteorological observations from two weather stations at elevations of 518 m a.s.l. and 593 m a.s.l. (He et al. 2021). Lapse rates of precipitation and temperature were derived from the two stations based on the station elevation. Meteorological forcing data was interpolated by the lapse rates and the HRU elevations to each HRU. Model performance was evaluated using the following metrics: *NSE* Eq. 1) is a commonly used metric for the evaluation of streamflow simulation, which compares the ratio between residual variance and observation variance, but it has the shortcoming in that it overemphasizes high flows (Krause et al. 2005). Therefore, the natural logarithmic *NSE* (*lnNSE*, Eq. 2) was additionally used to investigate model performance in simulating low flows. Mass bias (*MB*, Eq. 3) is a metric to evaluate the overall difference between simulation and observation mass or volume. Normalized Root Mean Square Error (*NRMSE*, Eq. 4) facilitates the comparison between model performance with different observation scales (e. g., observed SWE, ET and VWC in this study). Although *NSE* and *NRMSE* were calculated by similar equations, *NSE* is more suitable for the evaluation of variables such as streamflow that show large daily variability during the snowmelt and rainy seasons.

$$NSE = 1 - \frac{\sum (S_o - S_s)^2}{\sum (S_o - \overline{S_o})^2} \tag{1}$$

$$lnNSE = 1 - \frac{\sum (log(S_o) - log(S_s))^2}{\sum (log(S_o) - log(\overline{S_o}))^2} \tag{2}$$

$$MB = \frac{\sum S_s}{\sum S_o} - 1 \tag{3}$$

$$NRMSE = \frac{\sqrt{\frac{1}{n}\sum (S_o - S_s)^2}}{\overline{S_o}} \tag{4}$$

where S_o,S_s and $\overline{S_o}$ are the observed, simulated, and mean of the observed hydrological variables, respectively, and n is number of data samples. Simulated SWE, ET and VWC were evaluated only against observations on the forest site due to data availability.

3.3. Evaluation of hydrological sensitivity

Hydrological sensitivity in the SBF was quantified by the differences between the 13-year mean simulations in the ctrl and pgw scenarios forced by the WRF-CPM climate data. As the changes in soil properties and land cover such as disturbance caused by wildfire and harvest were not considered in the modelling scenarios, the simulations provide only the hydrological sensitivity driven directly by climate forcing changes.

Three types of variables were used to assess the hydrological sensitivity. The first type includes the water balance components of precipitation, ET, streamflow, and the snow accumulation, sublimation and melt processes. The second type are hydrological signatures such as the magnitudes and timing of maximum and minimum daily streamflow, annual runoff coefficients, the timing of the centre of mass for annual discharge (CMT), the snowcovered duration, and the timing of peak SWE before melt. A snow damming index was used to investigate changes in the role of snowpacks in storing precipitation over the winter season and releasing meltwater for spring runoff (López-Moreno et al., 2020). It indicates the difference between the cumulative fractions of precipitation and runoff (Eq. 5).

$$SI_d = \frac{\sum_{i=1}^{d} P_i}{P} * 100 - \frac{\sum_{i=1}^{d} Q_i}{Q} * 100 \tag{5}$$

where SI_d is the snow damming index on day-of-year (DOY) *d*. P and Q are the total annual precipitation and runoff, respectively. P_i and Q_i are precipitation and runoff on DOY *i*.

The last type is related to subsurface water, including the frozen soil depth, the durations of freezing and thawing seasons, soil moisture, the magnitudes of surface water infiltration, subsurface runoff, and groundwater. Assessments of the three types of hydrological variables were conducted separately in the west, central and east SBF. Spatial heterogeneity in hydrological sensitivity was thus assessed through the intercomparisons of the three SBF regions.

3.4. Uncertainty analysis

Uncertainty in the modelling results caused by model parameterizations of tree species, forest soil type, and the areal fraction of forest was analyzed one by one. The initial model setting (Section 3.2) was used as benchmark in the uncertainty analysis, in which, the tree species was Pine, soil type was sand and a forest areal fraction was 81.6%. To assess the uncertainty of the representation of tree species, the forest HRU in the virtual models was parameterized by Aspen and Spruce in two test model runs, respectively. Canopy parameters including LAI, vegetation height, and snow load capacity for Aspen and Spruce were used from He et al. (2021). The uncertainty of model simulations was then estimated as the percentage difference of the simulated hydrological variables between the test and benchmark model runs by Eq. (6).

$$U = \frac{M - m}{m} \times 100 \tag{6}$$

where M is the magnitude of a hydrological variable simulated by the test model run, and m is that simulated by the benchmark model run. Hydrological variables involved in the uncertainty analysis included mean annual streamflow, basin-average annual peak SWE, basin-average annual ET and soil moisture. Modelling uncertainty was assessed in the ctrl and pgw scenarios, respectively.

Similarly, to assess the uncertainty of soil type representation in the forest HRU, clay and loam soil types were parameterized in two test model runs. Porosity and hydraulic conductivity for these soil types were taken from Yu et al. (1993), Ritzema et al. (1996), and García-Gutiérrez et al. (2018). To assess the uncertainty of forest areal fraction, the percentage area coverage of the forest HRU was set to 50%, 70%, and 90% in three test model runs. The corresponding Fen HRU areal fraction was changed according to the test model settings, but the Open Water HRU coverage was fixed at 2.7%. The model uncertainty tests were only run at one virtual basin for each of the east, central and west zones, and the virtual basins were chosen based on their correspondence to the current median annual precipitation for each region.

4. Results

4.1. Model performance

Model simulations forced by measurements from meteorological

stations in the White Gull Creek basin were evaluated against observations in Fig. 2. The virtual basin model produced good performance for the simulation of streamflow in the period of Oct 2001 to Sep 2013 with *NSE* and *lnNSE* values of 0.61 and 0.72, respectively (Fig. 2a). The *MB* between the simulated and observed total streamflow was only −0.02 which is very good. Cumulative ET on the forest site tended to be overestimated by the model in the winter months of December to February in many years (Fig. 2b), resulting in a *NRMSE* value of 0.71; but the overall simulated ET in the entire modelling period was rather close to the overall observed ET, indicated by a small *MB* value of 0.1. Simulated SWE matched well with the observation on the forest site (Fig. 2c), indicated by the corresponding small *NRMSE* and *MB* values of 0.51 and 0.12. Simulated SWE was lower than observed in the winters of 2002 and 2006 but larger than observation in years of 2003–2004, 2007–2008 and 2012–2013, whilst showing good fit with observations in 2004–2005 and 2008–2012. The model simulation of the liquid VWC in the upper soil layer (0–60 cm) during May-September was evaluated against observations in Fig. 2d. Despite large differences between simulated VWC and observation during 2002 and 2003, the simulation matched well with observation in many years such as 2004, 2007, and 2012, resulting in overall *NRMSE* and *MB* values as small as 0.31 and 0.15.

The uncertainties introduced by using synthetic meteorological outputs from WRF during the current period of 2001–2013 to force the CRHM virtual basin model were investigated in Fig. 3. One would not expect synthetic weather forcing to necessarily produce hydrological outputs that match observations well, however the *NSE*, *lnNSE* and *MB* values show the streamflow simulations forced by the WRF ctrl data were only slightly less accurate than those forced by the station measurements (Fig. 3a). Simulated streamflow showed good agreement with baseflow observations in winter and early spring. The *NRMSE* between ET simulation forced by WRF ctrl data and observation was larger than that for ET simulated by station meteorological data (Fig. 3b), but the *MB* value was still lower than 0.2. In some water years such as 2003–2004 and 2006–2007, the cumulative ET simulations showed high agreements with the cumulative observations. Similar to Fig. 2c, in winters of 2002 and 2011, the simulated SWE were much lower than the observations (Fig. 3c); whilst SWE simulations matched the observations very well in most of the remaining winters. Small values of *NRMSE* and *MB* indicated even better performance in simulating soil liquid VWC when forced by the WRF ctrl data than forced by the station measurements (Fig. 3d). Overall, the WRF-CRHM model performance was sufficiently good to use as tool for further analysis.

4.2. Sensitivity of annual ET and streamflow

Changes in average annual mean air temperature, annual precipitation (*P*) between the two 13-year modelling periods across the SBF are

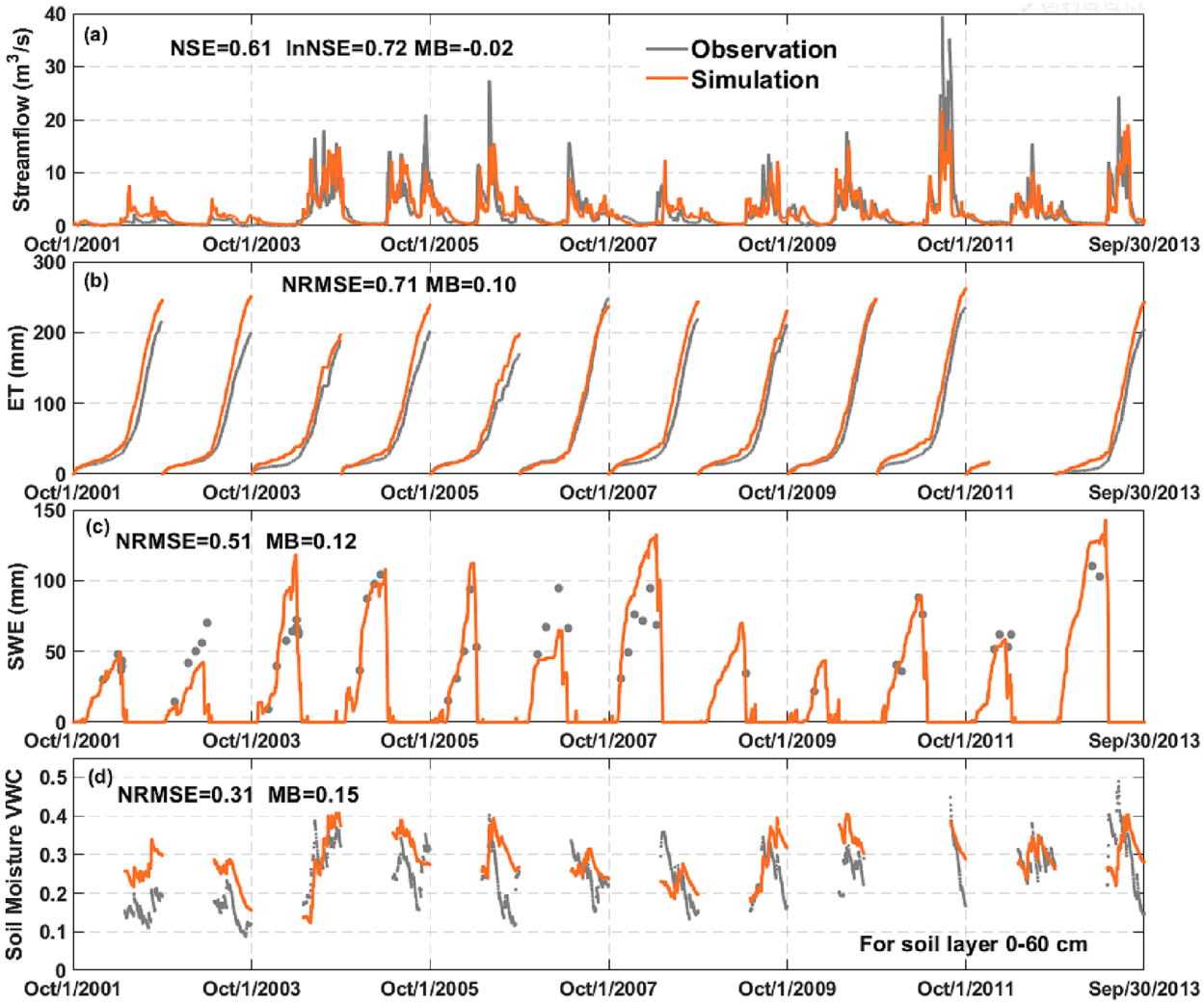

Fig. 2. Performance of the CRHM based virtual basin model in the WGC basin forced by meteorological station observations over 2001–2013, (a) for daily streamflow at the basin outlet, (b) for cumulative daily ET at the forest site, (c) for daily SWE at the forest site, and (d) for volumetric liquid water content (VWC) of upper soil layer during May-September at the forest site.

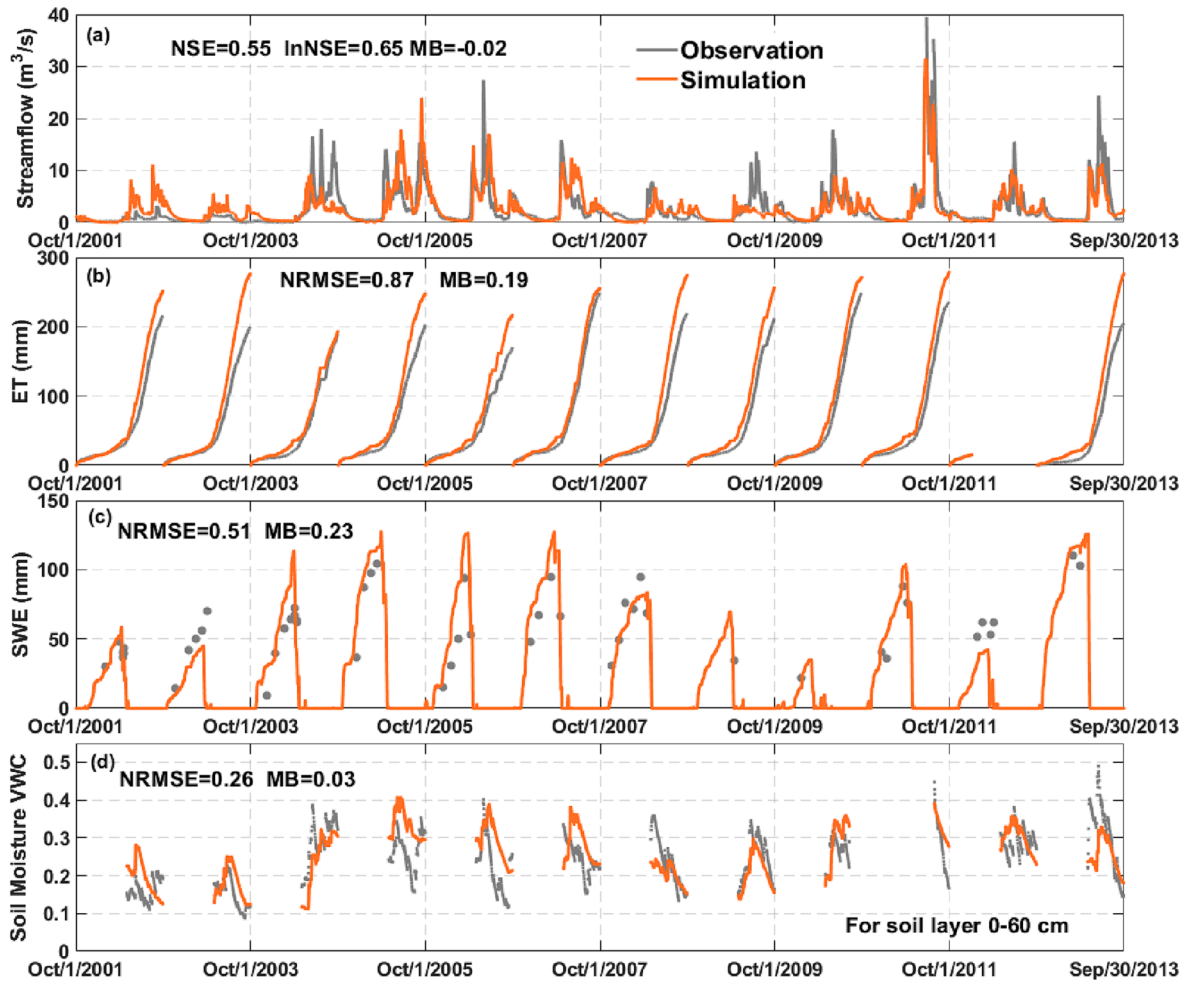

Fig. 3. Similar to Fig. 2, but for the performance of the CRHM-based virtual basin model forced by WRF climate simulations in the current period (ctrl).

presented in Fig. 4. Change in *P* refers to the percentage change in comparison to its mean annual value in the current scenario simulated by the WRF ctrl data. Fig. 4a shows that the SBF warmed by 4.5–7 ℃ by 2087–2099 (pgw) in comparison to 2001–2013 (ctrl). The central SBF, which is at relatively lower latitudes, would experience the greatest warming; whilst the west SBF would experience the smallest warming, and the east SBF only moderate warming. Meanwhile, annual *P* consistently rose across the SBF, apart from a few sites in the central region (Fig. 4b). The greatest increase in *P* would be around 38% in the east SBF. Annual *P* in the central SBF showed the smallest increase and some decreases of around −0.8% on its southern fringe. The west SBF showed large spatial variabilities in *P*: it increased by around 37% in the

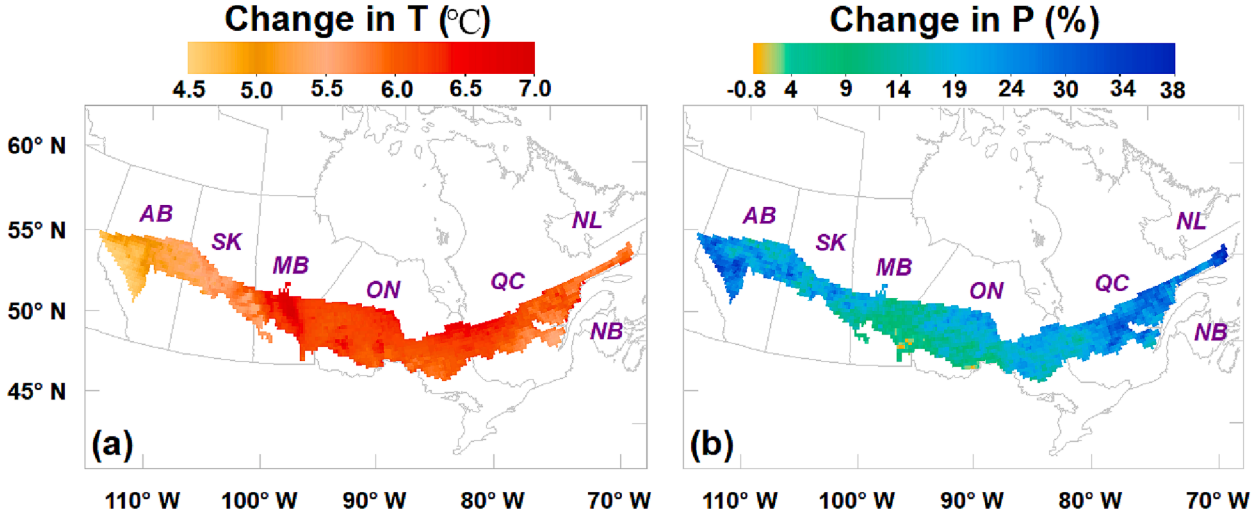

Fig. 4. Change in (a) annual mean air temperature with positive representing future warming, and the percentage future changes in (b) mean annual precipitation.

southwest SBF of Alberta, whilst increasing slightly in eastern Saskatchewan and western Manitoba.

Table 2 presents changes in the mean annual values over the three SBF regions and shows that averages of annual *P*, ET and streamflow over the 13-year modelling period increased in the pgw scenario in all the three SBF regions: On average, annual *P* in the east SBF would increase the most, by 253 mm (24%), whilst increasing by only 120 mm (21%) and 106 mm (15%) in the west and central SBF, respectively. Similarly, annual ET in the east SBF would increase notably by 56 mm (20%), but only slightly in the west and central SBF [11 mm (5%) and 17 mm (7%), respectively]. Annual streamflow forced by pgw scenario would be 64 mm (35%), 48 mm (17%) and 95 mm (16%) higher than currently in the west, central and east SBF, respectively. Fig. 5a-c show that *P* would increase mainly in March-July in the west and central regions, whilst *P* increases in winter (November-February) would be notable in the east. According to Fig. 5d-e, ET would increase in the freshet season from March to June but would slightly decrease over July-August in the west and central regions. The east ET would consistently increase in the growing season from April to October (Fig. 5f). Streamflow would mainly increase in the winter and spring seasons (October to June), but decrease in June-August (Fig. 5g-i), especially in the central and east regions. Reductions in streamflow and ET in summer were likely due in part to the reduced soil moisture which would result in lower subsurface runoff and forest transpiration. Fig. 5 indicates that the spatial variability of *P*, ET and streamflow in the east is larger than that in the west and central. The spatial variability of ET and streamflow in the central and east regions would increase from ctrl to pgw.

Fig. 5j-l indicate that the most pronounced decrease in streamflow exceedance probability would occur in the current spring melting period, March to May, indicating enhanced and earlier peak flows under pgw scenario. Conversely, the streamflow exceedance probability in summer (July to August) would increase substantially due to lower streamflows. The streamflow exceedance probability in late fall/early winter (November-December) would decrease substantially in the central SBF (Fig. 5k), indicating enhancement of a bimodal shape for hydrographs under pgw scenario. Shifts in the timing of minimum streamflow exceedance probability indicate that peak daily flows would more likely occur in spring rather than summer in the central and east SBF (Fig. 5j-l), but would still occur in late June in the west SBF (Fig. 5j). Small shifts in the timing of maximum streamflow exceedance probabilities in the west and central SBF show that annual low flows would still occur in late February to early March. In contrast, the timing of low flows in the east SBF would advance from early March to middle February under pgw scenario. Table 2 shows specific changes in the mean streamflow timing. In particular, the annual maximum daily flow would occur only 2 days earlier in the west, but about one month earlier in the central and east SBF. The date of annual low flows would advance by 15–22 days in the west and east SBF, but by only 3 days in the central.

Table 2
Mean changes (pgw - ctrl) in meteorological inputs, ET and streamflow regimes in the west, central and east SBF. Positive values indicate increases under the pgw scenario, whilst negative values indicate reductions or advances. Values in brackets show the percentage changes in the variables.

Variable	West	Central	East
Mean Annual air T (℃)	5.3	6.2	6.0
Annual P (mm)	120 (21%)	106 (15%)	253 (24%)
Annual total ET (mm)	11 (5%)	17 (7%)	56 (20%)
Annual streamflow (mm)	64 (35%)	48 (17%)	95 (16%)
Timing of maximum daily flow (day)	−2	−39	−26
Timing of minimum daily flow (day)	−15	−3	−22
Centre mass timing of annual streamflow (day)	−17	−27	−40
Annual maximum daily flow (mm)	0.3	−0.08	−0.8
Annual minimum daily flow (mm)	0.05	0.05	0.4
Annual runoff ratio	0.05	0.01	−0.04

Meanwhile, the timing of the centre of mass of annual streamflow volume would advance by 17 days in the west, 27 days in the central and 40 days in the east SBF, respectively. However, mean magnitude changes in the maximum and minimum daily flows would be less than 1 mm (Table 2). Basin-average annual runoff ratios (*Q*/*P*) would increase by 0.05 in the west but decrease by 0.04 in the east (Table 2) and would not change appreciably in the central SBF.

4.3. Sensitivity of snow processes

Under the pgw scenario, the mean annual snowfall would decrease by 50 mm (21%) in the central and by 109 mm (28%) in the east (Table 3), whilst it would only decrease by 8 mm (5%) in the west SBF. The greatest reduction in annual snow sublimation of 18 mm (38%) would occur in the east, in the central SBF it would be moderate (12 mm and 33%), whilst the west SBF would experience only a 7 mm (25%) reduction in snow sublimation. Similarly, the east SBF would experience the greatest declines in annual snowmelt, 90 mm (26%), and peak SWE, 89 mm (30%). In contrast, annual snowmelt in the west SBF would decrease slightly, by 2 mm (0.5%), and peak SWE in this region would only decrease by 3 mm (7%) – far smaller than these decreases for the central of 38 mm (19%) and 31 mm (19%), respectively, which themselves are smaller than that predicted for the east.

Comparisons of the daily snow processes in ctrl and pgw scenarios indicate that the first snowfall would occur half a month later and precipitation would shift to rainfall earlier (Fig. 6a-c), especially in the central and east regions. Accordingly, snow loss from sublimation would start in late November instead of October (Fig. 6d-f). Cumulative snow sublimation would reach its maximum in late March or early April in the pgw scenario, which is one month earlier than current. Although snowmelt would start only a few days earlier in the pgw scenario (Fig. 6g-i), it would cease about one month earlier in the central and east regions. The primary reason for this difference is the greater melt rate during April-May in the pgw scenario; and the second is that snow accumulation in the pgw scenario would be smaller (Fig. 6j-l). Under the ctrl scenario, the peak SWE date was late March in the west, early April in the central and late April in the east region. Under pgw scenario, the peak SWE date would advance to middle March in both central and east regions.

The mean snowcovered period would decline greatly under pgw: decreasing by 41 days in the west, 44 days in the central and 50 days in the east SBF (Table 3). Considering the current mean annual snowcovered durations were 187 days, 194 days, and 199 days in the west, central and east regions, respectively, the 41–50 days reduction means the snowcovered period would decline substantially, by 23%. The peak SWE date would advance by 17 days in the west, 18 days in the central and 25 days in the east SBF. Although this advance is less than 20 days in the west and central regions, it advanced the CMT of annual streamflow by 17–27 days (see Table 2), strongly impacting the spring freshet timing.

Fig. 7 compares the ratio of seasonal snowfall to annual *P* (snowfall ratio) and the ratio of sublimation to seasonal snowfall (sublimation ratio) in the three SBF regions. Under the ctrl scenario, the snowfall ratio in the west averaged 0.28 with a large range characterized by a maximum value 0.2 higher than its minimum (Fig. 7a). The current mean snowfall ratio in the west was lower than that in the central (0.33) and east (0.36) regions, reflecting lower winter precipitation amounts, but would become similar (around 0.22) in all regions in the future due to greater declines in snowfall (and increases in winter rainfall) in the east and central regions. Similarly, the sublimation ratio showed large spatial variability in the SBF (Fig. 7b), with differences between its maximum and minimum values up to 0.12. For the current climate, the mean sublimation ratio was 0.17 in the west and 0.16 in the central, which were larger than the value of 0.13 in the more humid east. For the future climate, the sublimation ratio would decrease to 0.11 in the east, and to around 0.14 in both west and central regions as a result of more

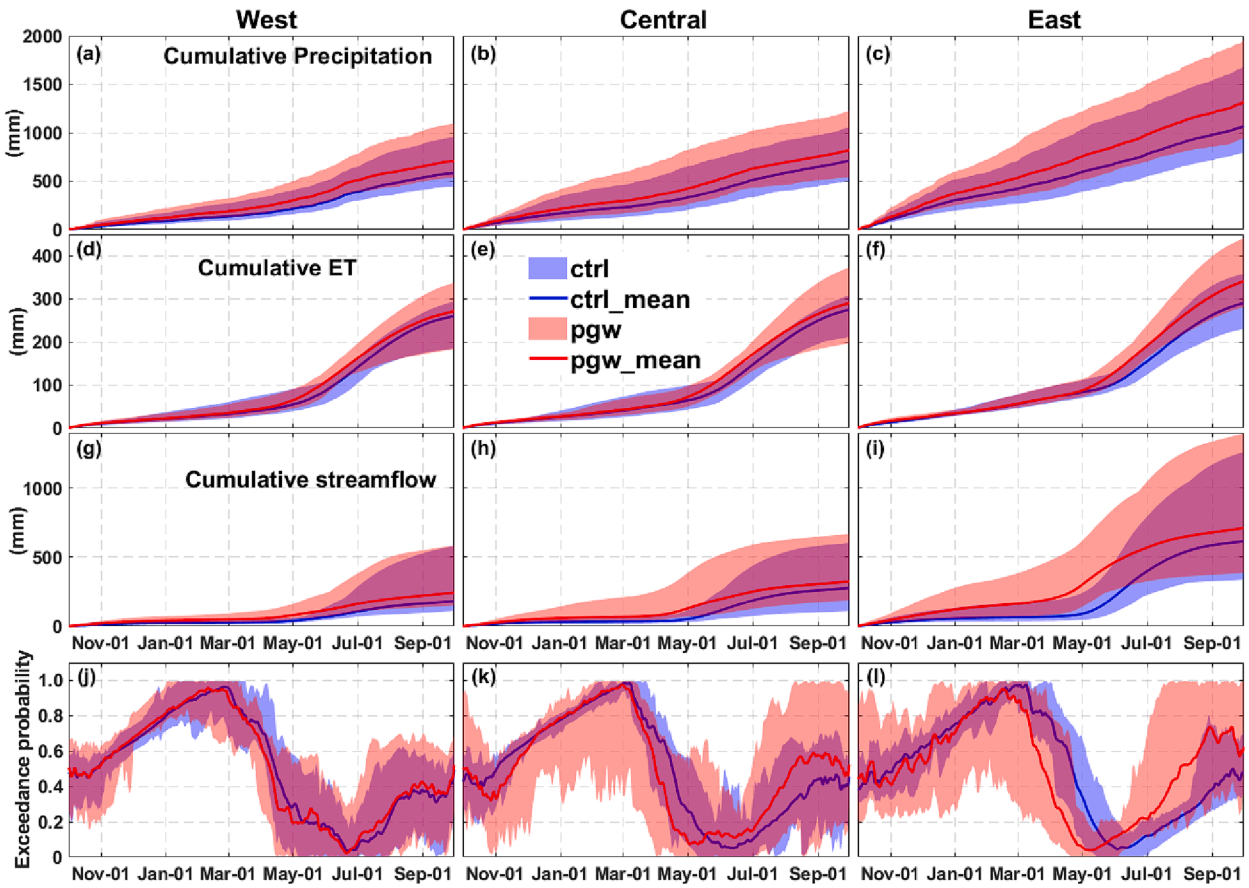

Fig. 5. Comparisons of the 13-year mean water balance components in the current (ctrl) and future (pgw) scenarios in the three SBF regions for water years starting Oct 1. (a-c) for cumulative precipitation, (d-f) for cumulative ET, (g-i) for cumulative streamflow, (j-l) for daily exceedance probabilities of mean daily streamflow where a low exceedance probability refers to peak flows and high probability to low flows. Bands refer to full range of the spatial variability and solid lines indicate mean values over the virtual basins in each region.

rapid unloading and melt of intercepted snow from forest canopies and shorter snowcovered seasons.

The snow damming index rose across the SBF from west to east, reflecting larger winter precipitation amounts in the east (Fig. 8). Currently (Fig. 8a-c), the snow damming index increased in the accumulation season, peaks around May 1st, and then declined to zero around August 1st in the west and around July 1st in the central and east SBF. In the future (Fig. 8d-f), the snow damming index would become much smaller over the SBF, peaking around April 1st, and then decreasing to zero around June 1st in the central and east SBF, but still lasting until around August 1st in the west. Declines in the snow damming index indicate a smaller role for snow hydrology in storing and releasing *P* in the future, especially in the east.

4.4. *Sensitivity of seasonally frozen soils and soil moisture*

For the current climate (Fig. 9a-c), SBF soils started freezing around October 10th and became completely frozen in December. After a 4-month frozen soil period, the soil started thawing around April 1st and thawed completely by August 1st. In the future, the soil would start freezing around two or three weeks later than currently and completely freeze only in January. The completely frozen duration would decline by around two months in the west and central, and by about three months in the east SBF. The onset of thaw would advance from late April and early May to mid-March across the SBF. Subsequently, soils would completely thaw before July 1st in the future climate. With reduced soil freezing and enhanced thawed periods, infiltration of rainfall and snowmelt would be much higher in the winter and melting seasons in the future climate (Fig. 9d-f). Meanwhile, ET from soil water in the unfrozen season of April-June would be strongly enhanced, presumably along with the primary productivity of the forest (Fig. 9g-i). The reduction in soil water ET in July-August can explain the reduction of total ET in Fig. 5d-e in the west and central regions, which can be attributed to the enhanced ET in April-June strongly reducing soil moisture availability for ET later in the summer. Subsurface runoff in both freezing and thawing seasons would increase in the future climate (Fig. 9j-l), because the reduced soil freezing and enhanced thawing would increase effective soil permeability for water movement. The timing of peak subsurface runoff would advance by one month in the central and east SBF, but not in the west. Similarly, reduction in the summer subsurface runoff in central and east in the future can be attributed to the reduced soil moisture availability caused by greater runoff in spring. The reduction in subsurface runoff was one of the main reasons for the future summer streamflow reduction in Fig. 5h-i.

On average, the annual mean depth of frost in soils would decrease by 10–14 cm (20–23%) across the SBF (Table 3). Annual infiltration would increase by 121 mm (33%) in the west, and by 145 mm (34%) and 339 mm (55%) in the central and east SBF, respectively. Annual ET from soil water would increase by 15 mm (9%) in the west, 24 mm (14%) in the central, and 65 mm (40%) in the east SBF. Mean annual subsurface runoff would increase by 58 mm (166%) in the west, and by 78 mm (107%) and 169 mm (64%) in the central and east SBF, respectively. Due to the enhanced effective soil permeability, percolation from soil and surface water into the groundwater reservoir would be enhanced in the future climate. The enhanced percolation would result in greater deep groundwater drainage (Table 3), because the increased recharge would

Table 3
Mean changes (pgw - ctrl) in snow and soil variables in the west, central and east SBF. Values in brackets show the percentage changes in the variables.

Variable	West	Central	East
Annual snowfall (mm)	−8 (-5%)	−50 (-21%)	−109 (-28%)
Annual snow sublimation (mm)	−7 (-25%)	−12 (–33%)	−18 (-38%)
Annual snowmelt (mm)	−2 (-0.5%)	−38 (-19%)	−90 (-26%)
Annual peak SWE (mm)	−3 (-7%)	−31 (-19%)	−89 (-30%)
Snow ratio to annual precipitation	−0.06	−0.10	−0.15
Duration snowcovered period (day)	−41 (–22%)	−44 (–23%)	−50 (-25%)
Timing of peak SWE (day)	−17	−18	−25
Annual mean frozen depth of soil (cm)	−11 (-20%)	−10 (–22%)	−14 (–23%)
Annual infiltration of surface water into soil (mm)	121 (33%)	145 (34%)	339 (55%)
Annual actual ET from soil water (mm)	15 (9%)	24 (14%)	65 (40%)
Annual subsurface runoff (mm)	58 (166%)	78 (107%)	169 (64%)
Mean soil moisture in the upper layer (mm)	−41	−38	−43
Mean soil moisture in the lower layer (mm)	−15	−16	6
Mean soil moisture in the total soil layer (mm)	−56 (-28%)	−54 (-27%)	−37 (-14%)
Mean deep groundwater drainage (mm)	50 (30%)	45 (25%)	108 (57%)
Ratio of infiltration to total rainfall and snowmelt	0.06	0.10	0.14
Ratio of annual actual ET from soil to infiltration	−0.11	−0.09	−0.02
Ratio of annual subsurface runoff to infiltration	0.11	0.10	0.02

exceed the storage capacity of the groundwater reservoir. The deep groundwater drainage would increase by 50 mm (30%), 45 mm (25%), and 108 mm (57%) in the west, central, and east regions, respectively, showing that much of the increased water surplus goes into deep groundwater drainage after the rather limited groundwater storage capacity is filled. Ratios in Table 3 indicate that the partitioning of total water inputs of rainfall and snowmelt to infiltration would increase by 0.06–0.14 over the SBF. The ratio of ET from soil water to the total infiltrated water would decrease by around 0.1 in the west and central, and by an insubstantial 0.02 in the east SBF. In contrast, the ratio of subsurface runoff to total infiltrated water would increase by around 0.1 in the west and central, and by around 0.02 in the east SBF.

Soil moisture in the SBF would decline in the future climate, as forced by increased ET and subsurface flow to streams, especially from the upper soil layer (Fig. 10a-c). In the upper layer, mean daily soil moisture would decrease by 41 mm in the west, and by 38 mm and 43 mm in the central and east SBF (Table 3), respectively. Soil moisture in the lower layer would change by relatively smaller amounts (Fig. 10d-f, Table 3); decreasing by 15–16 mm in the drier west and central regions and increasing by 6 mm in the wetter east. This can be partly attributed to the increased percolation from upper soil water along with the enhanced soil thawing and a longer thawed period. Soil moisture in the upper layer showed greater seasonal dynamics than that in the lower layer because upper layer soil moisture is the main source of water for transpiration. Total soil moisture would decrease by 56 mm (28%) and 54 mm (27%) in the west and central, and by a smaller 37 mm (14%) in the east SBF (Fig. 10g-i, Table 3). The mean daily soil moisture started to rise in May in the current climate, because of infiltration from snowmelt, and peaked in late June, after which the sum of ET and subsurface runoff began to exceed cumulative infiltration. In the future climate, the soil moisture would start to rise in April and peak in early June, due to earlier snowmelt, reduced soil freezing and enhanced thawing. The spatial variability of soil moisture in the west was larger than in the central and east in the current climate, but under climate change, the spatial variability of soil moisture in the west and central would decline, whilst expanding slightly in the east.

5. Discussion

5.1. Comparisons with previous studies

The two 13-year WRF-CPM outputs (current and pgw) used to force the sensitivity analysis in this work have proven effective for sensitivity investigation in a wide range of studies in Canada (e. g., Fang and Pomeroy, 2020; Krogh and Pomeroy, 2019; Li and Li, 2021). These studies have indicated that bias-corrected convection-permitting WRF ctrl outputs matched with surface meteorological observations reasonably well in western Canada. Considering the large area and limited availability of surface observations in SBF, bias-corrections to surface observations were not conducted for the WRF-CPM outputs here. In spite of that, results in this paper suggest that near surface meteorological outputs from the WRF ctrl simulation without bias-correction performed acceptably well in predicting observed streamflow, SWE, ET, and liquid soil water content in a well-gauged SBF basin, White Gull Creek. Meanwhile, the 4-km WRF-CPM outputs without bias-correction that were used have proven to outperform reanalysis data and CMIP5 ensemble outputs in balancing surface water budgets (Kurkute et al. 2020) and uniquely can represent extreme future hydrometeorological events (Li et al. 2019) in Canadian river basins with the lowest uncertainty available. Existing applications in western U.S. have shown good confidence in snowfall and snow accumulation estimated by the 4-km WRF-CPM simulations (Liu et al. 2017). In the absence of higher resolution climate model simulations across the SBF, the current 4-km WRF-CPM outputs appear to be one of the least uncertain sources of meteorological forcing for investigating hydrological sensitivity. While it is not as long as the WMO specified climate normal period (WMO, 2017), the 13-year WRF-CPM output contains historical extremes of flood and drought and so is extremely useful as it has no internal trends in an era of high non-stationarity.

Although it has become accepted practice to force hydrological models using multiple climate outputs from highly uncertain and biased RCMs and evaluate the modelling uncertainty from climate inputs, outputs from other climate models (and other RCP scenarios) were not used for model forcing in this study because of their typically coarse spatial resolution and large uncertainties in representing rain storms caused by convection in the SBF and large biases in seasonal temperature and precipitation (Rasouli et al., 2019). Here, to reduce uncertainty and bias and improve realism, only the WRF-CPM was used for the sensitivity assessment. The characteristics of WRF-CPM simulations are not inconsistent with outputs from other climate models. For example, simulations in the pgw RCP 8.5 scenario indicate a temperature (T) warming of up to 4.5 ℃ in the west and 7 ℃ in the central and east SBF. This result is comparable to the warming magnitudes reported by CMIP5 models in Bush and Lemmen (2019) who reported warming of up to 6.9 ℃ in Ontario and Quebec by the end of this century. The WRF pgw simulations suggested increases in annual precipitation of around 10–30% in Ontario and Quebec which are close to the estimated increases of 17–22% in Bush and Lemmen (2019). These results are also consistent with the estimates of four GCMs driven by the IPCC Emissions Scenarios in Price et al. (2013) who indicated average warming of 4–5 ℃ over the Canadian boreal zone. The mean annual precipitation in the east SBF by the end of this century estimated by GCMs in Price et al. (2013) was 1100–1200 mm which is close to but a bit lower than the estimation of around 1300 mm by the WRF pgw simulation. This may be due to the more realistic simulation of convection and precipitation recirculation by WRF. The WRF simulations estimated greater spatial variability in future climate changes over SBF than estimations in Bush and Lemmen (2019) and Price et al. (2013), benefiting from the high resolution of 4 km and improved microphysics for precipitation dynamics.

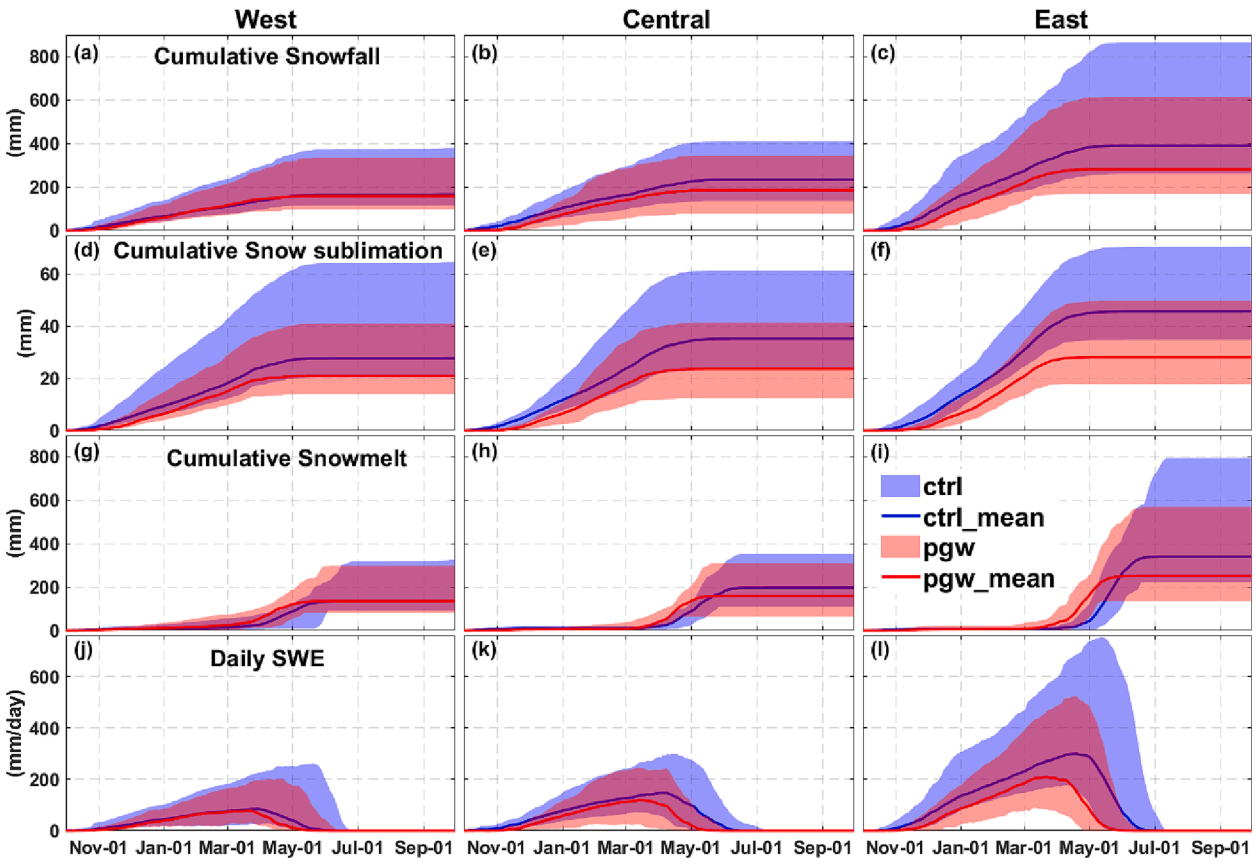

Fig. 6. Comparisons of the 13-year mean snow balance components in the ctrl and pgw scenarios in the three SBF regions. (a-c) cumulative snowfall, (d-f) cumulative snow sublimation, (g-i) cumulative snowmelt, and (j-l) daily snow water equivalent (SWE). Bands refer to full range of the spatial variability and solid lines indicate mean values over the virtual basins in each region.

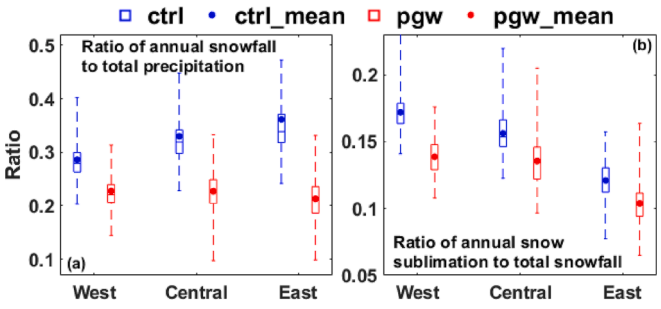

Fig. 7. Changes between ctrl and pgw in (a) snowfall ratio to total P, (b) ratio of snow sublimation to total snowfall. Whiskers of the boxplots refer to the full range of spatial variability in each of the three SBF regions. Dots indicate mean values over the virtual basins in each region.

Hydrological sensitivity estimated in this study is consistent with previous studies. Specially, the WRF-CRHM simulations yielded higher annual streamflow in most of the SBF when forced by the pgw outputs, which is similar to the findings in a mountain basin close to the southwest fringe of the SBF by Fang and Pomeroy (2020) and to a taiga basin north of the west SBF by Krogh and Pomeroy (2019). The enhanced annual ET associated with warmer *T* was generally supported by increased precipitation in most of the SBF. Surface water availability is expected to increase across the SBF in Quebec which is consistent with previous streamflow projections in 2080s by Minville et al. (2008 and 2010). The findings here that summer streamflow would decrease, winter streamflow would rise and the dates of onset spring snowmelt would advance are particularly consistent with the results forced by outputs from GCMs of the Canadian Centre for Climate modelling and analysis in Woo et al. (2008). Positive gradients from south to north in the future increases in *P*, ET and annual streamflow are evident across the SBF and are similar to findings shown by Guay et al. (2015) and CEHQ (2015).

Soil moisture showed a slightly decrease over the SBF in pgw scenario, indicating that the increased infiltration fails to offset enhanced ET, subsurface runoff and percolation to groundwater. The primary impact on soil moisture is on the upper layers which support tree and understorey root moisture withdrawals and also influence the near-surface duff moisture that is important for wildfire vulnerability and spread. Similarly, Dibike et al. (2017) projected enhanced magnitudes and frequency of soil water drought in western Canada using the medium (RCP 4.5) and high (RCP 8.5) emission scenarios based on the difference between precipitation and potential ET; Dai (2013) predicted up to 6% decrease in the SBF soil moisture during 2080–2099 compared to 1980–1999, using 11 CMIP5 models in the RCP4.5 emission scenario. The reduced available soil moisture could have strong impacts on the reforestation in clear-cut and wildfire burned sites (Elliott et al. 1998), and likely increase the occurrence of wildfire in the future. The ratio of actual ET from soil water to total infiltration of surface water declined in the pgw scenario, indicating that ET withdraw from soil would continue to be energy limited as suggested by Cook et al. (2014). The reduced soil frost also promotes increased generation of subsurface runoff and percolation of soil water into groundwater due to the increased effective permeability (Kurylyk et al. 2014).

5.2. *Modelling uncertainty*

CRHM was parameterized from field measurements in the well

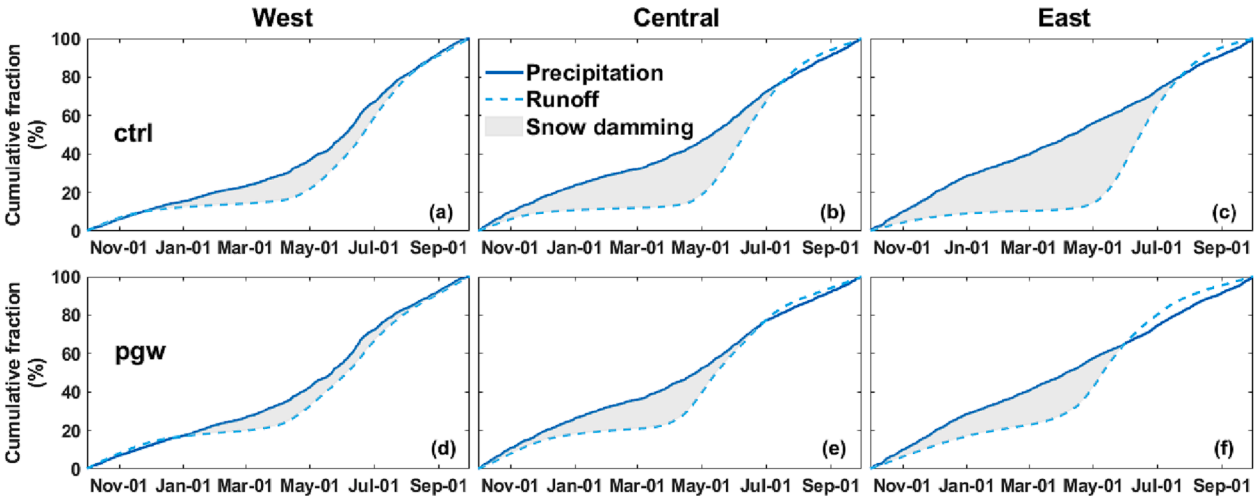

Fig. 8. Comparisons of the 13-year mean snow damming index in the ctrl and pgw scenarios in three SBF regions. Lines show mean values over the virtual basins in each region.

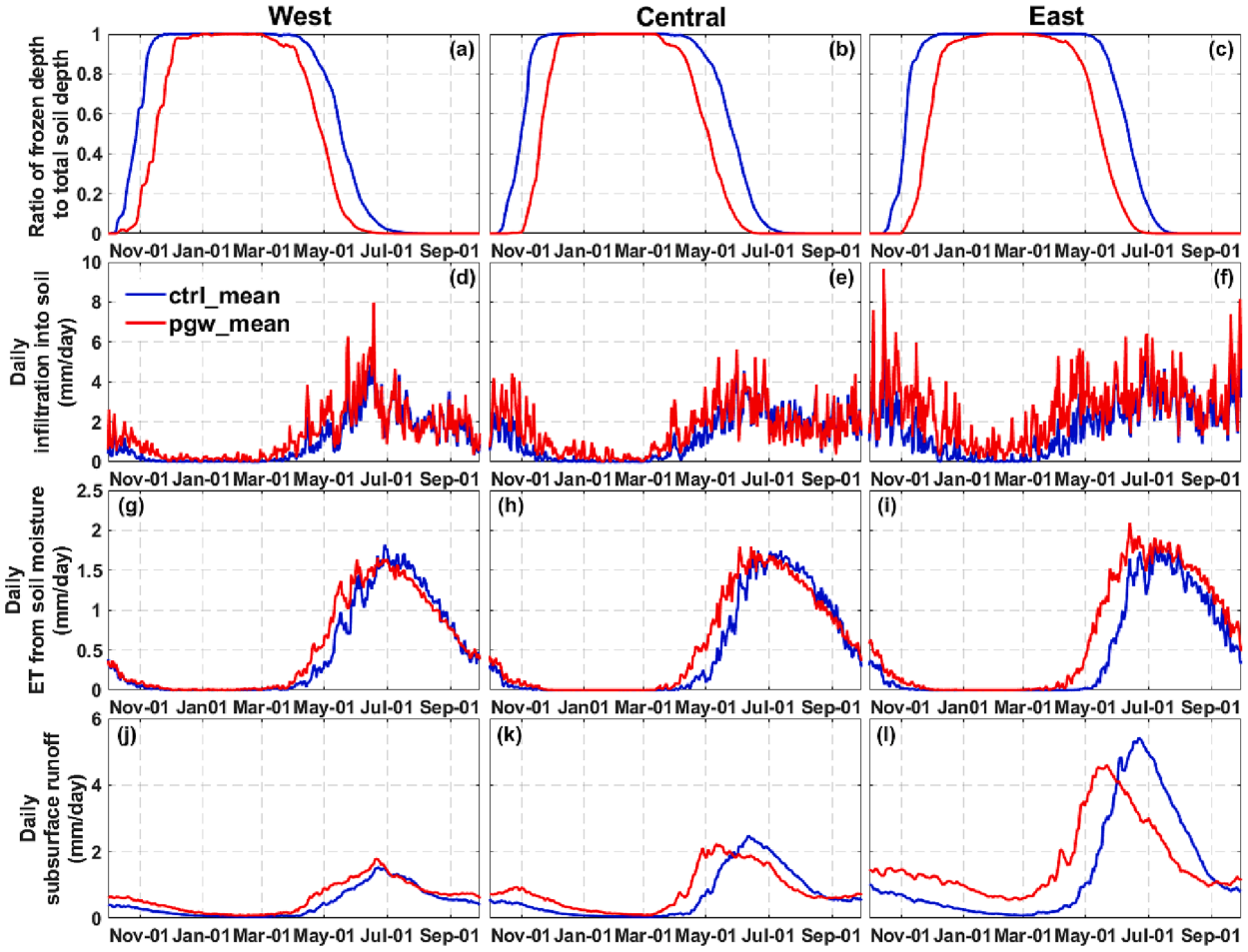

Fig. 9. Comparisons of the 13-year mean soil water variables in ctrl and pgw scenarios. (a-c) daily frozen soil depth fraction. (d-f) daily infiltration of snowmelt and rainfall into soil. (g-i) daily ET withdrawal from soil moisture. (j-l) daily subsurface runoff. Lines show mean values over the virtual basins in each region.

instrumented White Gull Creek basin in north-central Saskatchewan (Chen et al. 1997; Nijssen and Lettenmaier, 2002; Barr et al. 2012) without any calibration of parameters from streamflow observations. Basins in the SBF are generally level and homogeneous and their land surfaces are dominated by forest (Price et al. 2013). This provides a good foundation to set up virtual basins across the entire SBF for standardized and comparable hydrological modelling. Although hydrological modelling experiments in large-scale Canadian basins extracted by high resolution digital elevation models has been accomplished (Arheimer et al., 2020; Harrigan et al., 2020), hydrological modelling at large scale basins in the SBF is challenging because there are sparse observations of streamflow, evapotranspiration, soil moisture and snow cover data to

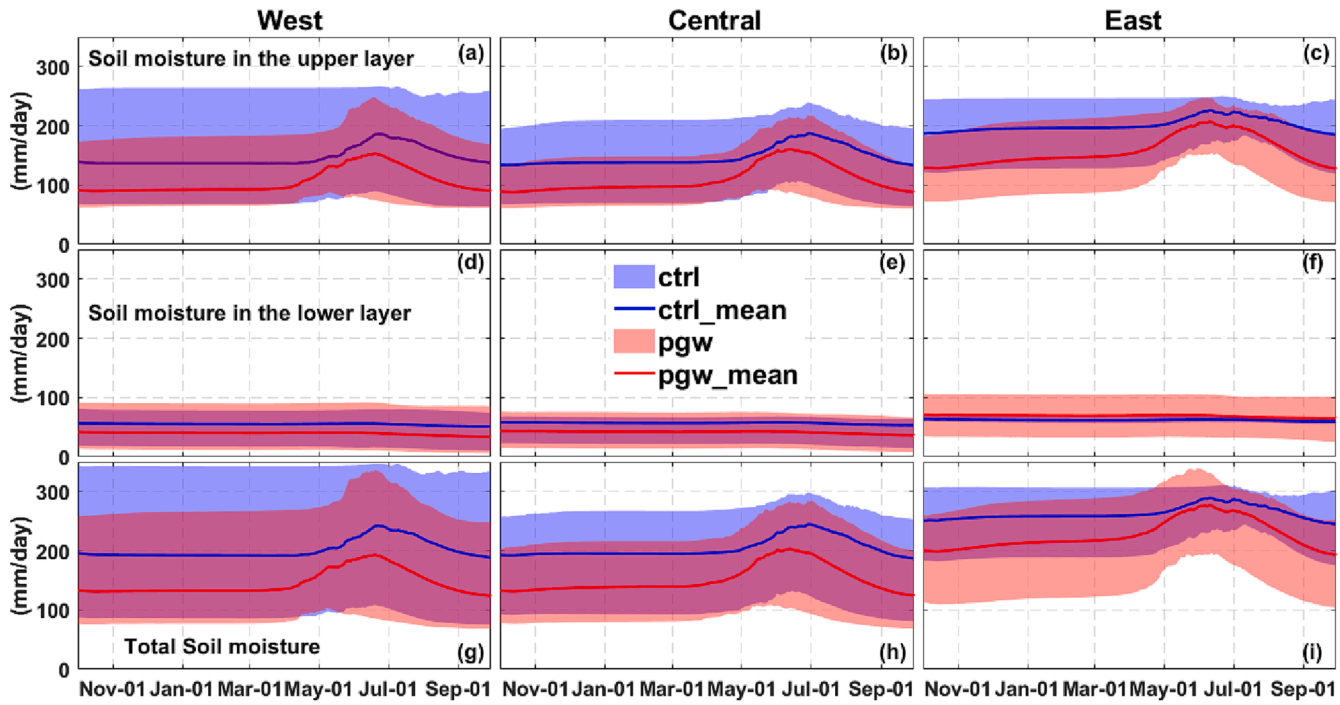

Fig. 10. Mean daily soil moisture in the three SBF regions forced by ctrl and pgw scenarios. (a)-(c) for upper layer with a soil depth range of 0–60 cm; (d)-(f) for lower layer with a soil depth range of 60–100 cm; and (g)-(i) for total soil moisture in the soil depth range of 0–100 cm. Bands refer to full range of the spatial variability and solid lines indicate mean values over the virtual basins in each region.

validate hydrological models over the SBF. Setting up CRHM-based models for larger basins will inevitably imply larger uncertainty as the model performance is hard to evaluate. There are also extensive and large lakes downstream of the SBF area, such as the Lake Winnipeg in Manitoba, Lake Nipigon and Superior in Ontario, which play significant roles in the drainage network and cause large uncertainty in delineating the extent of large basins over the SBF.

As the study aim is to compare hydrological sensitivity to future climate perturbation with respect to the spatial variability of climate over the SBF, the same land cover parameterisations were used for all virtual basins to exclude any impact of land cover variations on the sensitivity results. This approach has proven useful for comparing hydrological sensitivity at different locations in the extensive Canadian Prairies (Spence et al. 2022a,b; Armstrong et al. 2015). Moreover, the CRHM-based model was tested and validated by the land cover distribution in the WGC basin which NASA considered an exemplar of the SBF (Sellers et al. 1997). It is not possible to fully evaluate the model performance driven by different land cover distributions as no other site in the SBF is as well instrumented and observed as WGC. The WGC-based virtual basins were used as tools to assess hydrological sensitivity in upland headwaters forced by varied climate across the SBF, they are not real basins in the forest and so hydrological change must be considered relative and with respect to the water balance of the land cover components of the basin–forest, wetland and open water.

However, there are substantial spatial variabilities in land cover, soil, topography and geological features across the SBF. The variability of topography was considered in the model setting by using local elevation, latitude, longitude, slope and aspect in each virtual basin. Modelling uncertainty caused by land cover and soil parameterisations over the SBF was assessed in Table 4. In both ctrl and pgw scenarios, setting the tree species as Aspen simulated the largest annual streamflow, whilst the setting as Spruce resulted in the smallest. That can be explained by the greater ET and sublimation by Spruce because of its higher LAI. The percentage difference caused by the representation of tree species was up to 25% for annual streamflow in the west and up to 38% in the east, in comparison to the benchmark tree species setting of Pine. Uncertainty in simulation of SWE was close to that of annual streamflow, whilst that of simulated soil moisture was smaller (only up to 7% in the west). In contrast, the parameterisation of soil type in the forest site resulted in the largest uncertainty in the simulation of basin-average soil moisture (up to 31% in the west under the pgw scenario). The parameterisation of clay generated the highest soil moisture because of its smaller hydraulic conductivity, whilst the parameterisation of loam generated the lowest soil moisture. The greater soil moisture with clay parameters promoted greater transpiration and reduced streamflow volumes. Uncertainty of simulated streamflow and ET caused by the soil parameterisation were up to 13% in the west. Basin-average SWE showed insensitivity to the changes in soil type. These results are generally consistent with the findings of Marshall et al. (2021).

With the areal fraction of the Forest HRU ranging from 50% to 90%, the simulated annual streamflow volume can range from 48% greater than the benchmark simulation to 11% smaller. Uncertainty in simulated ET was as high as 17% in the east. Greater forest fractions resulted in smaller basin-average SWE due to the greater sublimation of canopy intercepted snowfall, and vice versa – a well documented effect in needleleaf forests (Pomeroy and Gray, 1995; Pomeroy et al. 2012). The 50% forest fraction generated an additional 13% snow accumulation than for the benchmark forest fraction of 81.6%. Basin-average soil moisture showed different responses to the increase of forest fraction in the ctrl and pgw scenarios; this can be partly attributed to the different changes in the soil moisture in Forest and Fen HRUs. Differences in the soil moisture simulation of up to 29% from the benchmark with changed forest fraction settings were observed. These modelling sensitivities and uncertainties should be taken into account when interpreting the climate sensitivity assessments in the context of real basins that are characterized by tree species, soil type and forest areal fractions that are different from the benchmark virtual basin model settings. The heterogeneity of geological and biological features could not be fully assessed due to limited data availability, but is suggested to have smaller impacts on the model simulations than variations in tree species, soil parameterizations and forest area coverage.

Table 4
Uncertainty (%) of the simulated hydrological variables caused by model parameterizations of tree species (Aspen, Pine, and Spruce), soil type (Clay, Loam, and Sand) and forest areal fraction (50–90%). # indicates the Number of selected representative virtual basins for the assessment in the west, central and east regions, respectively.

	Annual streamflow			Annual ET			Annual peak SWE			Soil Moisture		
	West (#1884)	Central (#260)	East (#592)	West (#1884)	Central (#260)	East (#592)	West (#1884)	Central (#260)	East (#592)	West (#1884)	Central (#260)	East (#592)
ctrl												
Aspen	25	15	13	–32	−36	−38	26	13	11	7	2	2
Pine (Benchmark)	0	0	0	0	0	0	0	0	0	0	0	0
Spruce	−8	−6	−5	12	14	15	−12	−5	−6	−4	−1	−1
Clay	−2	−2	−1	5	7	6	0	0	0	19	20	15
Loam	−2	−3	−2	5	7	6	0	0	0	−11	−11	−8
Sand (Benchmark)	0	0	0	0	0	0	0	0	0	0	0	0
forest fraction 50%	48	29	24	−16	−17	−16	13	6	5	−13	−11	−20
forest fraction 70%	16	10	8	−6	−6	−6	5	2	2	−1	2	−4
forest fraction 81.6% (Benchmark)	0	0	0	0	0	0	0	0	0	0	0	0
forest fraction 90%	−11	−5	−5	3	2	4	−3	−2	−1	−4	−11	−2
pgw												
Aspen	8	12	11	−25	−28	−29	22	10	10	6	−2	−2
Pine (Benchmark)	0	0	0	0	0	0	0	0	0	0	0	0
Spruce	−6	−5	−4	11	11	11	−9	−4	−3	−1	0	1
Clay	−13	−3	−2	11	6	5	0	0	0	31	12	18
Loam	1	−2	−1	2	3	4	0	0	0	−8	−8	−9
Sand (Benchmark)	0	0	0	0	0	0	0	0	0	0	0	0
forest fraction 50%	31	16	26	−10	−8	−17	13	5	5	29	25	−7
forest fraction 70%	4	11	9	−3	−8	−2	5	2	2	27	21	6
forest fraction 81.6% (Benchmark)	0	0	0	0	0	0	0	0	0	0	0	0
forest fraction 90%	−1	−2	0	4	3	5	−3	−1	−1	−10	−20	−13

5.3. Limitations

It is noted that climate change and associated ecological processes, forest management and harvesting will likely lead to changes in vegetation and soil parameters. For example, wildfire and insect outbreaks triggered by climate change could cause significant changes in the forest hydrological parameters. Land cover changes associated with forest disturbance from harvesting, disease and wildfire and lake-wetland evolution accompanying a warming climate should also be considered for comprehensive assessments of future hydrology (Boulanger et al., 2017). However, this work is only a sensitivity assessment based on headwater virtual basins in the SBF. Perturbations in vegetation and soil were not considered to focus on the hydrological sensitivity of primarily needleleaf and wetland uplands to climate change. A similar approach that used static land cover and soil parameters between ctrl and pgw scenarios in assessing hydrological variations was adopted in Fang and Pomeroy (2020). On the other hand, large water bodies such as large lakes and reservoirs, and exposed bedrock in the SBF regions were not addressed in the virtual basin model, because of their localized or regional occurrence and high spatial heterogeneity. The model results therefore have strong application to the hydrology of forest and wetland dominated upland regions in the SBF and have less certain applications to basins dominated by large lakes and groundwater outflow. When interpreting the virtual basin modelling results in real basins that have substantial local contributions of deep groundwater to streamflow, groundwater drainage should be routed to streamflow as baseflow, and changes in groundwater drainage should be added to changes in the overall streamflow. Beyond that, changes in soil properties across the forest caused by human activity and wildfire were assumed as negligible in this modelling experiment; wildlife activities such as beaver damming in the riparian areas serve important impacts on runoff routing in the forest (Stoll and Westbrook, 2020) but were not considered. The results thereby cannot be used to interpret spatially detailed future hydrological change of real basins in the SBF without referring to local vegetation, soils and hydrography and their transient responses to climate change. To involve all of these changes in realistic assessments of future hydrology will require more intensive collaborations between hydrologists, ecologists and forest managers, including assessment of the social drivers of forest change.

6. Summary and conclusions

This study simulated the major hydrological processes across the Canadian southern boreal forest (SBF, around 1.4 million km^2) using the Cold Regions Hydrological Modelling (CRHM) platform. The entire SBF was divided into 2243 upland virtual basins with an area of around 625 km^2 for each. The virtual basins were structured and parameterized in CRHM with the same land cover and hydrological parameters as the White Gull Creek (WGC) basin in order to compare the sensitivities of governing hydrological processes to climate variability and perturbation over the SBF. Near-surface outputs from the convection-permitting WRF simulations over the contiguous US (CONUS) at 4 km resolution for

current (ctrl, 2001–2013) and future climate scenarios (pgw, 2087–2099) were used to drive CRHM using distinct forcing for each of the 2243 virtual basins. Hydrological sensitivity across the entire SBF was then assessed and compared by difference between the CRHM simulations forced by WRF outputs in the ctrl and pgw scenarios. These results showed a profound spatial variability in hydrological sensitivity across the SBF:

Under the pgw scenario, mean temperatures would warm by 4.5℃ to 7℃ over the SBF, but the increased annual precipitation (*P*) would overwhelm the effects of warming on ET and sublimation and hence on runoff generation and so result in more streamflow over the SBF, especially in the west and east. The mean annual *P* would increase by 120 mm (21%) in the west and 253 mm (24%) in the east, while increasing by only 106 mm (15%) in the central SBF. Mean annual streamflow would increase by 64 mm (35%) and 95 mm (16%) in the west and east, and by 48 mm (17%) in the central SBF. More pronounced sensitivities in snow processes were found in the east than in the west and central SBF. In the pgw scenario, annual snowfall (peak SWE) would decrease by 109 mm (89 mm) in the east and by 8–50 mm (3–31 mm) in the west and central SBF. The snowcovered period would be shortened by 41–50 days over the SBF. The role of the seasonal snowpack in storing precipitation in the winter and releasing water in the spring would decline substantially, especially in the east SBF. Soil moisture would decrease across the SBF, driven by increased ET, subsurface runoff and enhanced soil thawing associated with shorter winters. On average, the annual mean soil moisture would decrease by 54–56 mm (around 27%) in the west and central and by 37 mm (14%) in the east SBF, with the most pronounced declines in near-surface soil moisture reserves that influence transpiration, primary productivity and wildfire risk. The larger sensitivity of streamflow and snow processes in the east SBF is partly due to the wetter climate and the larger increase in annual *P*, the later also buffered the sensitivity of soil moisture to warming.

These profound changes would make the SBF a rainier, less snow-dominated, higher water yield environment with greater primary productivity if it can retain its forest vegetation in the future. The shift to rainfall-runoff processes would mean a less reliable and predictable streamflow regime with possibly greater exposure to cycles of flood and drought with associated wildfire and disease risk. The distinct hydrological sensitivities in the west, central and east SBF suggested that particular and regional adaptation strategies corresponding to local climate are needed to deal with the effects of climate change. The greater sensitivities of streamflow and snowmelt in the east suggest more attention be paid to dealing with the higher risk of flooding than is needed in the west and central, whilst the larger changes in soil moisture in the west and central suggested more attention should be paid to sustaining available water for forest productivity than in the east. However, these results rely on the retention of the current needle-leaf forest cover in the SBF which itself is not certain due to harvesting, agricultural expansion, mining, disease and wildfires. The hydrological modelling outcomes here cannot be interpreted as future hydrological projections in real basins, as likely changes in land cover and soil parameters and local hydrography have not yet been considered.

Declaration of Competing Interest

The authors declare that they have no known competing financial interests or personal relationships that could have appeared to influence the work reported in this paper.

Data availability

Data will be made available on request.

Acknowledgement

The authors are grateful to Environment Canada and the University of Saskatchewan for long-term field studies in the Prince Albert Model Forest, BERMS sites and White Gull Creek basin and contributions by many scientists, technicians and students over several decades. Streamflow data collected from the Water Survey of Canada is also gratefully appreciated. Assistance on processing the meteorological outputs of WRF simulations by Xiao Ma and Dr. Yanping Li at University of Saskatchewan is gratefully acknowledged. Funding for this study came from the Canada First Research Excellence Fund's Global Water Futures programme through the Boreal Water Futures project, from the National Sciences and Engineering Research Council of Canada and the Canada Research Chairs program.

References

Agriculture and Agri-Food Canada, 2015. National ecological framework, Accessed 10 June 2016. [Available online at http://sis.agr.gc.ca/cansis/nsdb/ecostrat/index.html.].

Ahmed, H., Helgason, W., Barr, A., Black, T., 2020. Hydrometeorological observations at three boreal forest sites (aspen, jack pine, and black spruce) located in central Saskatchewan, Canada [Dataset]. Federated Research Data Repository. 10.20383/101.0292.

Arheimer, B., Pimentel, R., Isberg, K., Crochemore, L., Andersson, J.C.M., Hasan, A., Pineda, L., 2020. Global catchment modelling using World-Wide HYPE (WWH), open data, and stepwise parameter estimation. Hydrol. Earth Syst. Sci. 24, 535–559.

Armstrong, R.N., Pomeroy, J.W., Martz, L.W., 2015. Variability in evaporation across the Canadian Prairie region during drought and non-drought periods. J. Hydrol. 521, 182–195.

Ayers, H. D., 1959. Influence of soil profile and vegetation characteristics on net rainfall supply to runoff. Proceedings of Hydrology Symposium No.1: Spillway Design Floods, NRCC, Ottawa, 198-205.

Barr, A.G., van der Kamp, G., Black, T.A., McCaughey, J.H., Nesic, Z., 2012. Energy balance closure at the BERMS flux towers in relation to the water balance of the White Gull Creek watershed 1999–2009. Agric. For. Meteorol. 153, 3–13.

Boulanger, Y., Taylor, A.R., Price, D.T., Cyr, D., McGarrigle, E., Rammer, W., Sainte-Marie, G., Beaudoin, A., Guindon, L., Mansuy, N., 2017. Climate change impacts on forest landscapes along the Canadian southern boreal forest transition zone. Landscape Ecol. 32 (7), 1415–1431.

Brandt, J.P., 2009. The extent of the North American boreal zone. Environ. Rev. 17 (NA), 101–161.

Brandt, J. P., Flannigan, M. D., Maynard, D. G., Thompson, I. D., Volney, W. J. A., 2013. An introduction to Canada's boreal zone: Ecosystem processes, health, sustainability, and environmental issues. Environ. Rev. 21, 207–226.

Bush, E., Lemmen, D. S., 2019. Canada's Changing Climate Report; Government of Canada. Ottawa, editors, ON. 444 p.

CEHQ [Centre d'Expertise Hydrique Québec], 2015. Hydroclimatic atlas of southern Québec: The impact of climate change on high, low and mean flow regimes for the 2050 horizon; Centre d'expertise hydrique du Québec, Québec, Quebec, 81 p. <https://www.cehq.gouv.qc.ca/hydrome- trie/atlas/Atlas_hydroclimatique_2015EN.pdf>.

Changwei, X., Gough, W.A., 2013. A simple thaw-freeze algorithm for a multi-layered soil using the Stefan equation. Permafrost Periglac. 24 (3), 252–260.

Chen, J.M., Rich, P.M., Gower, S.T., Norman, J.M., Plummer, S., 1997. Leaf area index of boreal forests: Theory, techniques, and measurements. J. Geophys. Res. Atmos. 102 (24), 29429–29443.

Chow, V.T., 1964. Handbook of Applied Hydrology. McGraw-Hill, New York, p. 1495.

Clark, C.O., 1945. Storage and the Unit Hydrograph. T. Am. Soc. Civ. Eng. 110 (1), 1419–1446.

Cook, B.I., Smerdon, J.E., Seager, R., Coats, S., 2014. Global warming and 21st century drying. Clim. Dyn. 43 (9-10), 2607–2627.

Dai, A., 2013. Increasing drought under global warming in observations and models. Nat. Clim. Change 3 (1), 52–58.

Dibike, Y., Prowse, T., Bonsal, B., O'Neil, H., 2017. Implications of future climate on water availability in the western Canadian river basins. Int. J. Climatol. 37 (7), 3247–3263.

Ecological Stratification Working Group, 1996. A National Ecological Framework for Canada. Agriculture and Agri-Food Canada, Research Branch, Centre for Land and Biological Resources Research, and Environment Canada, State of the Environment Directorate, Ecozone Analysis Branch, Ottawa/Hull. Report and national map at 1: 7,500,000 scale.

Elliott, J.A., Toth, B.M., Granger, R.J., Pomeroy, J.W., 1998. Soil moisture storage in mature and replanted sub-humid boreal forest stands. Can. J. Soil Sci. 78 (1), 17–27.

Ellis, C.R., Pomeroy, J.W., Brown, T., MacDonald, J., 2010. Simulation of snow accumulation and melt in needleleaf forest environments. Hydrol. Earth Syst. Sci. 14, 925–940.

Ellis, C.R., Pomeroy, J.W., Essery, R.L.H., Link, T.E., 2011. Effects of needleleaf forest cover on radiation and snowmelt dynamics in the Canadian Rocky Mountains. Can. J. For. Res. 41 (3), 608–620.

Essery, R., Pomeroy, J., Ellis, C., Link, T., 2008. Modelling longwave radiation to snow beneath forest canopies using hemispherical photography or linear regression. Hydrol. Process. 22, 2788–2800.

Fang, X., Pomeroy, J., 2020. Diagnosis of future changes in hydrology for a Canadian Rocky Mountain headwater basin. Hydrol. Earth Syst. Sci. 24, 2731–2754.

Fang, X., Pomeroy, J.W., Westbrook, C.J., Guo, X., Minke, A.G., Brown, T., 2010. Prediction of snowmelt derived streamflow in a wetland dominated prairie basin. Hydrol. Earth Syst. Sc. 14, 991–1006.
Fang, X., Pomeroy, J.W., Ellis, C.R., MacDonald, M.K., Debeer, C.M., Brown, T., 2013. Multi-variable evaluation of hydrological model predictions for a headwater basin in the Canadian Rocky Mountains. Hydrol. Earth Syst. Sci. 17, 1635–1659.
García-Gutiérrez, C., Pachepsky, Y., Martín, M.Á., 2018. Technical note: Saturated hydraulic conductivity and textural heterogeneity of soils. Hydrol. Earth Syst. Sci. 22, 3923–3932.
Gelfan, A.N., Pomeroy, J.W., Kuchment, L.S., 2004. Modelling forest cover influences on snow accumulation, sublimation, and melt. J. Hydrometeorol. 5 (5), 785–803.
Gray, D.M., Toth, B., Zhao, L., Pomeroy, J.W., Granger, R.J., 2001. Estimating areal snowmelt infiltration into frozen soils. Hydrol. Process. 15 (16), 3095–3111.
Guay, C., Minville, M., Braun, M., 2015. A global portrait of hydrological changes at the 2050 horizon for the province of Québec. Can. Water Resour. J. 40 (3), 285–302.
Harding, R.J., Pomeroy, J.W., 1996. The energy balance of the winter boreal landscape. J. Climate 9 (11), 2778–2787.
Harrigan, S., Zsoter, E., Alfieri, L., Prudhomme, C., Salamon, P., Wetterhall, F., Barnard, C., Cloke, H., Pappenberger, F., 2020. GloFAS-ERA5 operational global river discharge reanalysis 1979-present, Earth Syst. Sci. Data. 12, 2043–2060.
He, Z., Pomeroy, J.W., Fang, X., Peterson, A., 2021. Sensitivity analysis of hydrological processes to perturbed climate in a southern boreal forest basin. J. Hydrol. 601, 126706.
Hedstrom, N.R., Pomeroy, J.W., 1998. Measurements and modelling of snow interception in the boreal forest. Hydrol. Processes 12 (10-11), 1611–1625.
Ireson, A.M., Barr, A.G., Johnstone, J.F., Mamet, S.D., van der Kamp, G., Whitfield, C.J., Michel, N.L., North, R.L., Westbrook, C.J., DeBeer, C., Chun, K.P., Nazemi, A., Sagin, J., 2015. The changing water cycle: the Boreal Plains ecozone of Western Canada. Wiley Interdiscip. Rev. Water 2 (5), 505–521.
Krause, P., Boyle, D.P., Base, F., 2005. Comparison of different efficiency criteria for hydrological model assessment. Adv. Geosci. 5, 89–97.
Krogh, S.A., Pomeroy, J.W., McPhee, J., 2015. Physically based mountain hydrological modelling using reanalysis data in Patagonia. J. Hydrometeorol. 16 (1), 172–193.
Krogh, S.A., Pomeroy, J.W., Marsh, P., 2017. Diagnosis of the hydrology of a small Arctic basin at the tundra-taiga transition using a physically based hydrological model. J. Hydrol. 550, 685–703.
Krogh, S.A., Pomeroy, J.W., 2019. Impact of future climate and vegetation on the hydrology of an Arctic Headwater Basin at the Tundra-Taiga Transition. J. Hydrometeorol. 20, 197–215.
Kurkute, S., Li, Z., Li, Y., Huo, F., 2020. Assessment and projection of the water budget over western Canada using convection-permitting weather research and forecasting simulations. Hydrol. Earth Syst. Sci. 24 (7), 3677–3697.
Kurylyk, B.L., MacQuarrie, K.T.B., McKenzie, J.M., 2014. Climate change impacts on groundwater and soil temperatures in cold and temperate regions: implications, mathematical theory, and emerging simulation tools. Earth-Science Rev. 138, 313–334.
La Roi, G.H., 1992. Classification and ordination of southern boreal forests from the Hondo-Slave Lake area of central Alberta. Can. J. Bot. 70 (3), 614–628.
Li, Y., Li, Z., 2021. High-Resolution Weather Research Forecasting (WRF) Modelling and Projection Over Western Canada, Including Mackenzie Watershed. Arctic Hydrology, Permafrost and Ecosystems, 815-847.
Li, Y., Li, Z., Zhang, Z., Chen, L., Kurkute, S., Scaff, L., Pan, X., 2019. High-resolution regional climate modelling and projection over western Canada using a weather research forecasting model with a pseudo-global warming approach. Hydrol. Earth Syst. Sci. 23 (11), 4635–4659.
Liu, C., Ikeda, K., Rasmussen, R., Barlage, M., Newman, A.J., Prein, A.F., Chen, F., Chen, L., Clark, M., Dai, A., Dudhia, J., Eidhammer, T., Gochis, D., Gutmann, E., Kurkute, S., Li, Y., Thompson, G., Yates, D., 2017. Continental-scale convection-permitting modelling of the current and future climate of North America. Clim. Dyn. 49 (1–2), 71–95.
López-Moreno, J.I., Pomeroy, J.W., Revuelto, J., Vicente-Serrano, S.M., 2013. Response of snow processes to climate change: Spatial variability in a small basin in the Spanish Pyrenees. Hydrol. Process. 27 (18), 2637–2650.
López-Moreno, J.I., Pomeroy, J.W., Alonso-González, E., Morán-Tejeda, E., Revuelto, J., 2020. Decoupling of warming mountain snowpacks from hydrological regimes. Environ. Res. Lett. 15 (11), 114006.
López-Moreno, J.I., Pomeroy, J.W., Morán-Tejeda, E., Revuelto, J., Navarro-Serrano, F. M., Vidaller, I., Alonso-González, E., 2021. Changes in the frequency of global high mountain rain-on-snow events due to climate warming. Environ. Res. Lett. 16 (9), 094021.
Luke, S.H., Luckai, N.J., Burke, J.M., Prepas, E.E., 2007. Riparian areas in the Canadian boreal forest and linkages with water quality in streams. Environ. Rev. 15 (NA), 79–97.
Marks, D., Kimball, J., Tingey, D., Link, T., 1998. The sensitivity of snowmelt processes to climate conditions and forest cover during rain-on-snow: a case study of the 1996 Pacific Northwest flood. Hydrol. Processes 12 (10-11), 1569–1587.
Marshall, A.M., Link, T.E., Flerchinger, G.N., Lucash, M.S., 2021. Importance of parameter and climate data uncertainty for future changes in boreal hydrology. Water Resour. Res. 57 (8).
Matasci, G., Hermosilla, T., Wulder, M.A., White, J.C., Coops, N.C., Hobart, G.W., Zald, H.S.J., 2018. Large-area mapping of Canadian boreal forest cover, height, biomass and other structural attributes using Landsat composites and lidar plots. Remote Sens. Environ. 209 (March), 90–106.
Maynard, D.G., Paré, D., Thiffault, E., Lafleur, B., Hogg, K.E., Kishchuk, B., 2014. How do natural disturbances and human activities affect soils and tree nutrition and growth in the Canadian boreal forest? Environ. Rev. 22 (2), 161–178.
Minville, M., Brissette, F., Leconte, R., 2008. Uncertainty of the impact of climate change on the hydrology of a nordic watershed. J. Hydrol. 358 (1-2), 70–83.
Minville, M., Krau, S., Brissette, F., Leconte, R., 2010. Behaviour and performance of a water resource system in Québec (Canada) under adapted operating policies in a climate change context. Water Resour. Manag. 24 (7), 1333–1352.
Monteith, J. L., 1965. Evaporation and environment. In State and Movement of Water in Living Organisms. 19th Symposium of the Society for Experimental Biology. Cambridge University Press: Cambridge; 205-234.
Nelson, T.A., Coops, N.C., Wulder, M.A., Perez, L., Fitterer, J., Powers, R., Fontana, F., 2014. Predicting climate change impacts to the Canadian boreal forest. Diversity 6 (1), 133–157.
Nijssen, B., Lettenmaier, D.P., 2002. Water balance dynamics of a boreal forest watershed: White Gull Creek basin, 1994–1996. Water Resour. Res. 38 (11), 37-1–37-12.
Pomeroy, J. W., Gray, D. M., 1995. Snowcover Accumulation, Relocation and Management, Science Report No. 7. National Hydrology Research Institute, Saskatoon, Environment Canada. 144 p.
Pomeroy, J. W., Granger, R., Pietroniro, A., Elliott, J., Toth, B., Hedstrom N., 1999. Classification of the boreal forest for hydrological processes, in Proceedings of the Ninth International Boreal Forest Research Association Conference, edited by S. Woxholtt, pp. 49–59, Aktuelt fraskogforskningen, Norsk institutt for skogforskning, Norw. For. Res. Institute, Oslo.
Pomeroy, J.W., Fang, X., Rasouli, K., 2015. Sensitivity of snow processes to warming in the Canadian Rockies. Proceedings, 72nd Eastern Snow Conference, 72, pp.22:23.
Pomeroy, J., Fang, X., Ellis, C., 2012. Sensitivity of snowmelt hydrology in Marmot Creek, Alberta, to forest cover disturbance. Hydrol. Process 26, 1891–1904.
Pomeroy, J.W., Granger, R.J., 1997. Sustainability of the western Canadian boreal forest under changing hydrological conditions — I: snow accumulation and ablation. In: Rosjberg, D., Boutayeb, N., Gustard, A., Kundzewicz, Z., Rasmussen, P. (Eds.), Sustainability of Water Resources Under Increasing Uncertainty. International Association Hydrological Sciences Publ No 240. IAHS Press, Wallingford, UK, pp. 207–242.
Pomeroy, J.W., Marks, D., Link, T., Ellis, C., Hardy, J., Rowlands, A., Granger, R., 2009. The impact of coniferous forest temperature on incoming longwave radiation to melting snow. Hydrol. Process. 23 (17), 2513–2525.
Pomeroy, J.W., Brown, T., Fang, X., Shook, K.R., Pradhananga, D., Armstrong, R., Harder, P., Marsh, C., Costa, D., Krogh, S.A., Aubry-Wake, C., Annand, H., Lawford, P., He, Z., Kompanizare, M., Lopez Moreno, J.I., 2022. The Cold Regions Hydrological Modelling Platform for hydrological diagnosis and prediction based on process understanding. J. Hydrol. 615, 128711.
Pomeroy, J.W., Li, L., 2000. Prairie and Arctic areal snow cover mass balance using a blowing snow model. J. Geophys. Res. 105 (D21), 26619–26634.
Pomeroy, J.W., Fang, X., Marks, D.G., 2016. The cold rain-on-snow event of June 2013 in the Canadian Rockies — characteristics and diagnosis. Hydrol. Process. 30 (17), 2899–2914.
Pomeroy, J.W., Schmidt, R.A., 1993. The use of fractal geometry in modelling intercepted snow accumulation and sublimation. Proc. Eastern Snow Conference 50, 1–10.
Pomeroy, J.W., Gray, D.M., Shook, K.R., Toth, B., Essery, R.L.H., Pietroniro, A., Hedstrom, N., 1998a. An evaluation of snow accumulation and ablation processes for land surface modelling. Hydrol. Process. 12 (15), 2339–2367.
Pomeroy, J.W., Parviainen, J., Hedstrom, N., Gray, D.M., 1998b. Coupled modelling of forest snow interception and sublimation. Hydrol. Process. 12 (15), 2317–2337.
Pomeroy, J.W., Gray, D.M., Hedstrom, N.R., Janowicz, J.R., 2002. Prediction of seasonal snow accumulation in cold climate forests. Hydrol. Process. 16 (18), 3543–3558.
Pomeroy, J.W., Gray, D.M., Brown, T., Hedstrom, N.R., Quinton, W.L., Granger, R.J., Carey, S.K., 2007. The cold regions hydrological model: a platform for basing process representation and model structure on physical evidence. Hydrol. Process. 21 (19), 2650–2667.
Price, D.T., Alfaro, R.I., Brown, K.J., Flannigan, M.D., Fleming, R.A., Hogg, E.H., Girardin, M.P., Lakusta, T., Johnston, M., McKenney, D.W., Pedlar, J.H., Stratton, T., Sturrock, R.N., Thompson, I.D., Trofymow, J.A., Venier, L.A., 2013. Anticipating the consequences of climate change for Canada's boreal forest ecosystems1. Environ. Rev. 21 (4), 322–365.
Priestley, C.H.B., Taylor, R.J., 1972. On the assessment of surface heat flux and evaporation using large-scale parameters. Mon. Weather Rev. 100 (2), 81–92.
Rasmussen, R., Liu, C., 2017. High Resolution WRF Simulations of the Current and Future Climate of North America. Research Data Archive at the National Center for Atmospheric Research, Computational and Information Systems Laboratory. 10.5065/D6V40SXP.
Rasouli, K., Pomeroy, J.W., Janowicz, J.R., Carey, S.K., Williams, T.J., 2014. Hydrological sensitivity of a northern mountain basin to climate change. Hydrol. Process. 28 (14), 4191–4208.
Rasouli, K., Pomeroy, J.W., Janowicz, J.R., Williams, T.J., Carey, S.K., 2019. A long-term hydrometeorological dataset (1993–2014) of a northern mountain basin: Wolf Creek Research Basin, Yukon Territory, Canada. Earth Syst. Sci. Data 11, 89–100.
Ritzema H. P., Kselik, R., Chanduvi, F. 1996. Drainage of Irrigated Lands. FAO Irrigation Water Management Training Manual No. 9, Food and Agriculture Organization of the United Nations: Rome, Italy; 74.
Sellers, P., Hall, F., Margolis, H., Kelly, B., Baldocchi, D., den Hartog, G., Cihlar, J., Ryan, M.G., Goodison, B., Crill, P., Ranson, K.J., Lettenmaier, D., Wickland, D.E., 1995. The boreal ecosystem-atmosphere study (BOREAS): an overview and early results from the 1994 field year. Bull. Am. Meteorol. Soc. 76 (9), 1549–1577.
Sellers, P.J., Hall, F.G., Kelly, R.D., Black, A., Baldocchi, D., Berry, J., Ryan, M., Ranson, K.J., Crill, P.M., Lettenmaier, D.P., Margolis, H., Cihlar, J., Newcomer, J., Fitzjarrald, D., Jarvis, P.G., Gower, S.T., Halliwell, D., Williams, D., Goodison, B.,

Wickland, D.E., Guertin, F.E., 1997. BOREAS in 1997: Experiment overview, scientific results, and future directions. J. Geophys. Res. 102 (D24), 28731–28769.
Shook, K., Pomeroy, J., 2011. Synthesis of incoming shortwave radiation for hydrological simulation. Hydrol. Res. 42, 433.
Sicart, J.E., Essery, R.L.H., Pomeroy, J.W., Hardy, J., Link, T., Marks, D., 2004. A sensitivity study of daytime net radiation during snowmelt to forest canopy and atmospheric conditions. J. Hydrometeorol. 5 (5), 774–784.
Spence, C., He, Z., Shook, K., Mekonnen, B., Pomeroy, J., Whitfield, C., Wolfe, J., 2022a. Assessing hydrological sensitivity of grassland basins in the Canadian Prairies to climate using a basin classification–based virtual modelling approach. Hydrol. Earth Syst. Sci. 26, 1801–1819.
Spence, C., He, Z., Shook, K., Pomeroy, J., Whitfield, C., Wolfe, J., 2022b. Assessing runoff sensitivity of North American Prairie Pothole Region basins to wetland drainage using a basin classification–based virtual modelling approach. Hydrol. Earth Syst. Sci. 26, 5555–5575.
Stoll, N.L., Westbrook, C.J., 2020. Beaver dam capacity of Canada's boreal plain in response to environmental change. Sci. Rep. 10, 1–12.
Verseghy, D.L., 1991. CLASS-A Canadian land surface scheme for GCMs. I. soil model. Int. J. Climatol. 11 (2), 111–133.
Weber, M.G., Flannigan, M.D., 1997. Canadian boreal forest ecosystem structure and function in a changing climate: Impact on fire regimes. Environ. Rev. 5 (3–4), 145–166.
Williams, T.J., Pomeroy, J.W., Janowicz, J.R., Carey, S.K., Rasouli, K., Quinton, W.L., 2015. A radiative–conductive–convective approach to calculate thaw season ground surface temperatures for modelling frost table dynamics. Hydrol. Process. 29 (18), 3954–3965.
WMO-No 1203, 2017. WMO Guidelines on the Calculation of Climate Normals. In Purpose. Chairperson, Publications Board World Meteorological Organization (WMO), Geneva, Switzerland.
Wong, J.S., Razavi, S., Bonsal, B.R., Wheater, H.S., Asong, Z.E., 2017. Inter-comparison of daily precipitation products for large-scale hydro-climatic applications over Canada. Hydrol. Earth Syst. Sci. 21 (4), 2163–2185.
Woo, M.K., Thorne, R., Szeto, K., Yang, D., 2008. Streamflow hydrology in the boreal region under the influences of climate and human interference. Philos. Trans. R. Soc. B Biol. Sci. 363 (1501), 2251–2260.
Yu, C., Cheng, J., Jones, L., Wang, Y., Faillace, E., Loureiro, C., Chia, Y., 1993. Data Collection Handbook to Support Modelling the Impacts ofRadioactive Material in Soil; No. ANL/EAIS-8; Argonne National Lab: Argonne, IL, USA.
Zhang, Z., Li, Y., Chen, F., Barlage, M., Li, Z., 2020. Evaluation of convection-permitting WRF CONUS simulation on the relationship between soil moisture and heatwaves. Clim. Dyn. 55 (1–2), 235–252.
Zhou, J., Pomeroy, J.W., Zhang, W., Cheng, G., Wang, G., Chen, C., 2014. Simulating cold regions hydrological processes using a modular model in the west of China. J. Hydrol. 509, 13–24.